



Ferric ions accumulate in the walls of metabolically inactivating *Saccharomyces cerevisiae* cells and are reductively mobilized during reactivation

| | |
|-------------------------------|---|
| Journal: | <i>Metallomics</i> |
| Manuscript ID | MT-ART-03-2016-000070.R1 |
| Article Type: | Paper |
| Date Submitted by the Author: | 16-Apr-2016 |
| Complete List of Authors: | Wofford, Joshua; Texas AandM University, Department of Chemistry Park, Jinkyu; Texas AandM University, Department of Chemistry McCormick, Sean; Texas AandM University, Department of Chemistry Chakrabarti, Mrinmoy; Texas AandM University, Department of Chemistry Lindah, Paul A; Texas AandM University, Department of Chemistry |
| | |

1
2
3
4
5
6
7
8
9
10
11
12
13
14
15
16
17
18
19
20
21
22
23
24
25
26
27
28
29
30
31
32
33
34
35
36
37
38
39
40
41
42
43
44
45
46
47
48
49
50
51
52
53
54
55
56
57
58
59
60

Ferric ions accumulate in the walls of metabolically inactivating *Saccharomyces cerevisiae* cells and are reductively mobilized during reactivation

Joshua D. Wofford,¹¶ Jinkyu Park,^{1,⊥,¶} Sean P. McCormick,^{1,§}¶ Mrinmoy Chakrabarti,^{1,⊤} and

Paul A. Lindahl ^{*,1,2}

¹From the Department of Chemistry, Texas A&M University, College Station, TX 77843 USA

²Department of Biochemistry and Biophysics, Texas A&M University, College Station, TX 77843 USA

*To whom corresponding should be addressed: Paul A. Lindahl, Department of Chemistry, Texas A&M University, College Station TX 77843-3255. Phone, 979-845-0956 ; Fax, 979-845-4719, email: lindahl@chem.tamu.edu.

[⊥]Current address: Nuclear Chemistry Research Division, Korea Atomic Energy Research Institute, Daejeon, 305-353, Republic of Korea

[§]Current address: Department of Chemistry, Ferris State University, Big Rapids MI 49307, United States

[⊤]Current address: Office of Research and Economic Development, University of Idaho, Moscow, ID, 83844, United States

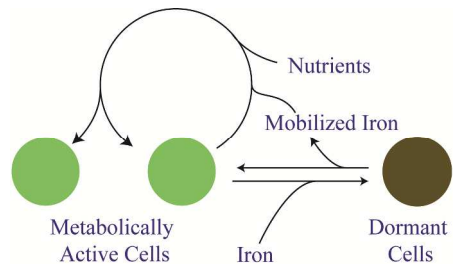
¶Contributed equally

Keywords: Mössbauer spectroscopy; electron paramagnetic resonance; Mathematical modeling; iron; Fit1, Fit2, Fit3.

1
2
3
4
5
6
7
8
9
10
11
12
13
14
15
16
17
18
19
20
21
22
23
24
25
26
27
28
29
30
31
32
33
34
35
36
37
38
39
40
41
42
43
44
45
46
47
48
49
50
51
52
53
54
55
56
57
58
59
60

Table of Contents Entry

Yeast cells accumulate large quantities of ferric ions in their cell walls as they become metabolically inactive. This Fe can be reduced and mobilized as cells become metabolically active.



Abstract

Mössbauer and EPR spectra of fermenting yeast cells before and after cell wall (CW) digestion revealed that CWs accumulated iron as cells transitioned from exponential to post-exponential growth. Most CW iron was mononuclear nonheme high-spin (NHHS) Fe^{III} , some was diamagnetic and some was superparamagnetic. A significant portion of CW Fe was removable by EDTA. Simulations using an ordinary-differential-equations-based model indicated that cells accumulate Fe as they become metabolically inactive. When dormant Fe-loaded cells were metabolically reactivated in Fe-deficient bathophenanthroline disulfonate (BPS)-treated medium, they grew using Fe that had been mobilized from their CWs AND using trace amounts of Fe in the Fe-deficient medium. When grown in Fe-deficient medium, Fe-starved cells contained the lowest cellular Fe concentrations reported for a eukaryotic cell. During metabolic reactivation of Fe-loaded dormant cells, Fe^{III} ions in the CWs of these cells were mobilized by reduction to Fe^{II} , followed by release from the CW and reimport into the cell. BPS short-circuited this process by chelating mobilized and released Fe^{II} ions before reimport; the resulting $\text{Fe}^{\text{II}}(\text{BPS})_3$ complex adsorbed on the cell surface. NHHS Fe^{II} ions appeared transiently during mobilization, suggesting that these ions were intermediates in this process. In the presence of chelators and at high pH, metabolically inactive cells *leached* CW Fe; this phenomenon probably differs from metabolic mobilization. The iron regulon, as reported by Fet3 levels, was not expressed during post-exponential conditions; Fet3p was maximally expressed in exponentially growing cells. Decreased expression of the iron regulon and metabolic decline combine to promote CW Fe accumulation.

Significance to Metalloomics

Fungal cells such as yeast contain a cell wall that plays important cellular functions and is responsible for the virulence of pathogenic fungi. We report here that the cell wall accumulates massive amounts of iron when cells become metabolically inactive. Cell wall iron is found mainly as magnetically isolated Fe^{III} ions. When such cells become metabolically reactivated, the cell wall Fe^{III} becomes reduced to Fe^{II} and released from the wall. Once mobilized in this way, the Fe^{II} ions can be imported into the cell and used for growth.

Introduction

Although commonly considered an *extracellular* structure, the cell wall (CW) is actually an *intracellular* component of fungal cells (1-4). It is synthesized from cellular components that are under the genetic control of the cell - about 20% of the genes in *Saccharomyces cerevisiae* affect CW construction (5, 6) – and the CW contributes to the cell's ability to survive and flourish. The CW provides structural support and rigidity, and it allows the cell to withstand high osmotic pressure. The CW allows cells to adhere to each other and to solid supports, and is involved in mating and morphogenesis (3). It affects the virulence of pathogenic fungi and thus has biomedical importance (7-11).

The CW of budding yeast *S. cerevisiae* consists of an inner glucan frame linked to an outer layer of mannose-based glycoproteins (12-15). The frame includes chitin and β -1,3-glucans. Numerous mannose-based glycoproteins are in the outer layer, most of which have N-linked glycosidic bonds anchored to the frame via β -1,6-glucan glycosylphosphatidylinositol (GPI) phosphodiester linkages (6). Mature GPI-CW proteins are linked to the frame via their C-termini. Their N-termini extend outward into the environment due to extensive glycosylation of serine and threonine residues in this region.

About 80% of the proteins in the CW can be solubilized using SDS, implying that such proteins are not covalently linked to the frame (1-6). Most covalently linked manno-proteins are solubilized by gluconase. Other CW proteins are attached to the frame via poorly defined “alkali-sensitive linkages”; these proteins dissociate from the frame under alkali conditions.

The CW constantly remodels as cells grow and divide, and its composition changes with the phase of the cell cycle and growth conditions. The CW acts like a filter to limit access of environmental species to cellular regions within the plasma membrane. Cell *porosity* refers to the

1
2
3 degree to which such species pass through the CW and into the cytosol. CW porosity maximizes
4
5 in the early-exponential phase of growth, and declines dramatically during post-exponential
6
7 growth (2). Declining porosity is associated with increasing densities of mannan side-chains and
8
9 disulfide bonds of the gluconase-solubilizable proteins of the outer layer. Porosity is not affected
10
11 by the more abundant SDS-solubilizable mannoproteins.
12
13
14

15 From the energy-dispersive TEM spectrum, Vainshtein *et al.* identified iron-containing
16
17 nanoparticles associated with the CW of yeast cells grown on medium containing high
18
19 concentrations of iron (16). X-ray microanalyses suggested that these particles are ferric oxides.
20
21 To the best of our knowledge, this is the only published physical characterization of CW iron in
22
23 yeast. Philpott and coworkers determined that ca. 40% of cellular iron is released upon treatment
24
25 with Zymolyase (17), a mixture of β -1,3-gluconase and proteases that catalyzes the disassembly
26
27 of the CW and releases mannoproteins (18). This implies that a large percentage of cellular Fe
28
29 can be found in the CW. The pH of the growth medium influences the amount and speciation of
30
31 metals that accumulate in the CW (19).
32
33
34
35

36 The only *S. cerevisiae* CW proteins known to be involved in Fe metabolism are the
37
38 “Facilitator of Iron Transport” mannoproteins Fit1, Fit2 and Fit3 (17). These proteins are
39
40 secreted by the cell and bound to the frame by β -1,6-glucan units through GPI anchors. They
41
42 contain numerous serine and threonine residues that are heavily glycosylated. FIT1/2/3 genes are
43
44 part of the Aft1/2-associated *Iron Regulon* (20). These genes are transcribed under Fe-deficient
45
46 growth conditions but not under Fe-rich ones. Their expression levels change dramatically (60 to
47
48 230 fold) depending on the concentration of Fe in the medium (17). Strains lacking these
49
50 proteins have difficulty importing Fe^{III} siderophores whereas the import rates of other Fe^{III}
51
52 complexes are unaffected. Thus, the Fit1/2/3 proteins facilitate import of *specific* siderophores,
53
54
55
56
57
58
59
60

1
2
3 rather than all Fe-species that enter the cell. Fit1/2/3-deficient strains behave as though they are
4 Fe-deficient even in Fe-replete medium, another indication that these proteins help import Fe.
5
6 Less CW Fe is found in Fit-deficient strains, again suggesting that the Fit proteins are involved
7
8 in Fe import (17). However, other Fe import proteins must also be involved. Fit proteins
9
10 apparently do not affect CW porosity.
11
12
13
14

15 Iron is an essential component of all eukaryotic cells. In yeast cells, environmental Fe
16 must pass through the CW on its way to the cell interior. Much cytosolic Fe is trafficked to the
17 mitochondria where it is used in the biosynthesis of iron-sulfur clusters (ISCs) and heme centers
18 (21). Many such centers are installed into respiratory complexes contained within that organelle.
19
20 Under Fe-sufficient and Fe-excess conditions, Fe traffics into vacuoles for storage (22).
21
22 Mitochondria and vacuoles are the two established “hubs” of Fe trafficking in yeast (23).
23
24
25
26
27
28

29 We recently reported that glucose-grown *S. cerevisiae* cells accumulate Fe in post-
30 exponential stages of growth (24). Based on the spectral characteristics of the Fe that
31 accumulated, we hypothesized that this Fe localized in vacuoles and/or mitochondria as
32 mononuclear nonheme high-spin (NHHS) Fe^{III} species and nanoparticles. At that time, we were
33
34 unaware that the CW accumulates Fe. Once aware of this, we wondered whether the
35
36 accumulated Fe in post-exponential cells might have actually localized in the CW rather than (or
37
38 in addition to) vacuoles. In this paper, we show that this is indeed the case. Our results suggest
39
40 that there are multiple types of Fe^{III} species in the CW, and that CW Fe accumulates when
41
42 metabolic activity is declining. CW Fe^{III} is reductively mobilized and released from
43
44 metabolically reactivated cells. Some of the resulting Fe^{II} ions are reimported into such cells to
45
46 support growth. The concentration of CW Fe is high, far greater than that found within the
47
48 cytosol and internal organelles, indicating that the CW is a third “hub” in fungal iron trafficking.
49
50
51
52
53
54
55
56
57
58
59
60

Methods

Yeast Strain and Media. W303-1B (*MAT α* , *ura3-1*, *ade2-1*, *trp1-1*, *his3-11,15*, *leu2-3,112*) cells were grown from frozen stocks on standard YPAD agar plates for 3-4 days. The medium contained 1% yeast extract, 2% peptone, 2% (w/v) glucose and 40 mg/L adenine hemisulfate dihydrate. Single colonies were used to inoculate YPD medium. YPD-grown cells were used to inoculate synthetic minimal medium (*MM*) prepared as described (25) with 40 μ M $^{57}\text{Fe}^{\text{III}}$ citrate added (24). We will refer to this medium as $^{57}\text{Fe}_{40}\text{B}_0$, where the superscript indicates the Fe isotope used, the first subscript indicates the final concentration of added Fe-citrate in μ M, and the last subscript indicates the final concentration (also in μ M) of added bathophenanthroline disulfonate (BPS). The Fe^{II} chelator BPS is commonly used to generate Fe-deficient medium. Other MM-based media used include $^{56}\text{Fe}_{40}\text{B}_0$, $^{57}\text{Fe}_1\text{B}_{21}$, Fe_0B_{30} , $\text{Fe}_0\text{B}_{100}$, Fe_0B_0 , and $\text{Fe}_0\text{B}_{100}$ -*NAB* (Table S1). *NAB* indicates medium prepared with No Amino acids or Bases. Sterile deionized water (DW) was also used as a medium into which cells were inoculated.

Fe-loaded and Fe-starved cells. A colony was used to inoculate 50 mL of YPD medium, and cells were grown in a shaker at \sim 150 rpm and 30 $^{\circ}$ C until $\text{OD}_{600} = 1.0$. An aliquot was transferred to $^{57}\text{Fe}_{40}\text{B}_0$ medium, achieving $\text{OD}_{600} = 0.01$. Cells grown for 5 days will be called *Fe-loaded* or *post-exponential*. Another aliquot was added to $^{57}\text{Fe}_1\text{B}_{21}$ medium, again attaining $\text{OD}_{600} = 0.01$. Cells harvested after 15 hrs ($\text{OD}_{600} \approx 1.0$) or 5 days will be called *Fe-starved*.

Cell manipulations and spectroscopy. Cells were harvested by spinning at 2,500 \times g for 5 min. Cells were washed 3 times with chilled 100 μ M EDTA in 150 μ M Tris pH 8.0 followed by 3 washings with chilled DW. Resulting cells were packed into 5 mm OD tubes by centrifugation at

1
2
3 4,000×g for 5 min using an ultracentrifuge (Beckman Coulter Optima L-90K) and swinging-
4 bucket rotor (SW 32 Ti). For metal analysis, packed cells were resuspended with an equal
5 volume of DW. Resulting suspensions were incubated overnight in 200 μL of 30% trace-metal
6 grade HNO₃ (Fisher Scientific) at 95 °C, and then diluted with DW before analysis. Fe
7 concentrations were measured by ICP-MS (Agilent 7700x) as described (26). A cell packing
8 efficiency of 70% was used (27). Western Blots were performed as described (24).
9

10
11 For Mössbauer (MB) studies, cells were loaded into MB cups by centrifugation at
12 5,000×g for 5 min and frozen in liquid N₂. MB spectra were collected on either a model MS4
13 WRC or LHe6T spectrometer (SEE Co., Edina, MN). Both instruments were calibrated using α-
14 Fe foil at RT. For UV-vis studies, packed cells were diluted with an equal volume of DW and
15 then transferred to a 2 mm pathlength quartz cuvette (NSG Precision Cells, Inc.). Spectra were
16 recorded on a Hitachi 3010 spectrometer possessing a Head-On photomultiplier tube.
17 Absorbances were measured 6 times and results were averaged and multiplied by 5 to yield the
18 value expected if a 10 mm rather than a 2 mm path-length cuvette had been used.
19
20
21
22
23
24
25
26
27
28
29
30
31
32
33
34
35
36
37
38

39 **Dissolved O₂ concentrations:** An O₂ probe (24" long FOXY-T-1000-RTD, Ocean Optics Inc,
40 Dunedin FL) was placed in an iron-free custom glass/titanium bioreactor filled with 24 L of
41 ⁵⁷Fe₄₀B₀ medium at 30 °C. The reactor was inoculated with cells that had been grown overnight
42 in YPAD similarly supplemented. Standard purity O₂ gas was bubbled into the bioreactor at a
43 fixed rate of ca. 500 mL/min. The paddle stir-rate was ca. 100 RPM.
44
45
46
47
48
49
50
51
52

53 **Measuring CW Fe release.** Cells were grown in the bioreactor for 5 days and then centrifuged
54 and washed twice with water to remove residual medium. Cells were resuspended in water and
55
56
57
58
59
60

1
2
3 aliquots were transferred into 50 mL plastic screw-top vials. The vials were centrifuged to yield
4 pellets the volumes of which (ca. 5 mL) were determined from the height of the pellet and the
5 mass of water needed to fill the vial to that height (after the experiment). The volume of the
6 pellet was corrected for packing efficiency. Various treatment buffers (40 mL) were added to
7 each tube at time 0, including: water, 100 μ M EDTA (prepared in 150 μ M Tris buffer pH 8.0),
8 and 100 μ M EDTA plus lyticase (Sigma; 1000 U of lyticase activity per gram of wet packed cell
9 in tube) in SP buffer (1.2 M sorbitol in 50 mM potassium phosphate pH 7.4). At 10 min
10 intervals, 2 mL of solution were removed from each tube and transferred to microfuge tubes and
11 centrifuged. Supernatants were saved for metal analysis and pellets were washed twice with
12 triple-distilled water or SP buffer (lyticase samples) that lacked chelators or lyticase. The
13 volumes of these pellets and supernatants were measured, and Fe, Mn, Cu, and Zn concentrations
14 were determined. At each buffer condition, the relationship $V_{\text{pell}} \cdot [\text{Fe}_{\text{pell}}] + V_{\text{sup}} \cdot [\text{Fe}_{\text{sup}}]$ equalled a
15 constant number of moles at each time point within an error of $\pm 10\%$.

34 Results and Discussion

37 **Mössbauer and EPR characterization of iron-loaded post-exponential cells before and after**
38 **CW digestion.** Iron accumulates in glucose-grown yeast cells as they transition from exponential
39 to post-exponential growth (24). To test whether that Fe accumulated in the CW, we grew WT
40 cells in $^{57}\text{Fe}_{40}\text{B}_0$ medium and harvested them during exponential ($\text{OD}_{600} = 0.2, 0.4, \text{ and } 0.7$) and
41 post-exponential ($\text{OD}_{600} = 1.5$, 5 days after inoculating) growth phases. Cells were washed 3
42 times with water, 100 μ M EDTA, or EDTA plus lyticase, an enzyme that, like zymolyase,
43 digests CWs.

54 Low-temperature (5 K), low-field (0.05 T) MB spectra of cells harvested at different
55 times during exponential phase and washed in water (Figure 1, A and B) were similar to each
56
57
58
59
60

1
2
3 other and to previous spectra of cells harvested in this growth phase (24). Exponential cells
4 washed with EDTA exhibited similar spectra (data not shown). Spectra were dominated by a
5
6 sextet due to NHHS Fe^{III} in the vacuole (Figure 1, green line) followed by a central quadrupole
7
8 doublet (gold line) due mainly to [Fe₄S₄]²⁺ clusters and LS Fe^{II} heme centers in mitochondria
9
10 (28). Minor quadrupole doublets due to HS Fe^{II} heme (orange line) and NHHS Fe^{II} (purple line)
11
12 were also evident. The average concentration of Fe in these samples was 370 ± 170 μM. Cellular
13
14 Mn, Cu and Zn concentrations were also determined (Table 1). A portion of freshly harvested
15
16 exponentially grown cells were treated with lyticase, but this had no significant effect on the
17
18 spectrum (Figure 1C), suggesting that little if any Fe accumulated in the CWs of exponentially
19
20 growing cells.
21
22
23
24
25

26
27 The MB spectrum of cells harvested 5 days after inoculation, in post-exponential mode,
28
29 exhibited a percent effect 10-times greater than that of cells harvested during exponential growth
30
31 (Figure 1D, black trace). Subsequent ICP-MS analysis indicated that such cells were indeed
32
33 loaded with Fe (Table 1). Cells from the same harvest but treated with lyticase/EDTA and then
34
35 washed 3 times with SP buffer afforded a MB spectrum (Figure 1, D and F, blue traces) that was
36
37 only ca. 10% as intense as that of water-washed cells. Similar cells treated with EDTA alone
38
39 exhibited a spectrum (Figure 1, D and E, red line) that was less intense than water-washed cells
40
41 but more intense than those washed with lyticase/EDTA.
42
43
44
45

46 After the MB spectra of Figure 1 (and Figures 4 and 5, see below) were collected,
47
48 samples were pulverized and packed into EPR tubes while being kept in or directly above liquid
49
50 N₂. The 10 K X-band EPR spectrum of post-exponential cells showed dramatic changes upon
51
52 lyticase/EDTA treatment (Figure 2, A vs. C). The spectrum of the water-washed sample (Figure
53
54 2A) exhibited intense features at g = 4.3 and in the g = 2 region. The g = 4.3 signal is typical of
55
56
57
58
59
60

1
2
3 paramagnetic NHHS Fe^{III} species with rhombic symmetry. The signal in the g = 2 region was
4
5 unusually broad as is typical of Fe^{III} oxyhydroxide nanoparticles found in mitochondria of yeast
6
7 that are defective in ISC-related processes (29-31). The intensity at g = 4.3 was significantly
8
9 diminished and the broad g = 2 signal was absent in the spectrum of the lyticase/EDTA-treated
10
11 sample (Figure 2C). The EPR spectrum of the sample treated only with EDTA (Figure 2B) was
12
13 also devoid of the broad g = 2 signal and the integrated intensity of the sharper g = 4.3 derivative
14
15 signal was reduced relative to that in the spectrum of water-washed cells. The decline in the
16
17 intensity of these signals upon lyticase treatment suggests that CW Fe is heterogeneous, with
18
19 mononuclear NHHS Fe^{III} affording the g = 4.3 signal and superparamagnetic Fe^{III} nanoparticles
20
21 affording the broad g = 2 signal.
22
23
24
25
26

27 The concentration of cellular Fe after lyticase-treatment was about 24% of that in water-
28
29 washed cells (Table 1). Interestingly, the concentrations of Mn, Cu, and Zn did *not* increase in
30
31 post-exponential cells, relative to concentrations of the same metals in exponential cells, and the
32
33 concentrations of the same metals did not decline upon lyticase treatment. We conclude that *Fe*
34
35 *(but not Cu, Mn, or Zn) accumulates in the CW of post-exponential (but not exponential) cells*
36
37 *and that the majority (75% - 90%) of the Fe in those cells is located in the CW.*
38
39
40
41
42

43 **Rate of O₂-dependent metabolism declines in post-exponential cells.** To evaluate whether
44
45 post-exponential cells are metabolically active, we simultaneously measured cell density, as
46
47 reported by OD₆₀₀, and dissolved [O₂] in the growth medium *vs.* time after inoculating 24 L of
48
49 minimal medium with cells that had been grown overnight in YPAD. [O₂] consumption was used
50
51 as a reporter of metabolic activity. O₂ gas was bubbled into the bioreactor at a fixed rate, with
52
53 temperature and stir conditions also fixed. The resulting OD₆₀₀ trace (Figure 3, green dots)
54
55
56
57
58
59
60

exhibited a lag phase followed by exponential growth and then a transition into the post-exponential state. The corresponding traces of dissolved $[O_2]$ (Figure 3, red dots) began high (because the reactor contained few cells and the bubbling rate was fast) and then declined as the concentration of cells and O_2 consumption increased (overpowering the fixed bubbling rate). Towards the end of the experiment, dissolved $[O_2]$ gradually returned to near its initial concentration.

This final return of $[O_2]$ to near its initial concentration indicated that metabolically active cells converted into an inactive dormant state when nutrients became scarce. We assumed this in a chemical model (Figure 3, bottom and Table 2) in which metabolically active cells ($Cell_A$) self-replicate and metabolize O_2 along with a hypothesized nutrient N. Dormant cells ($Cell_D$) were assumed only to convert into active cells when $[N]$ levels were sufficiently high. This model was translated into ordinary differential equations (ODEs) [1] – [4].

$$\frac{d[Cell_A]}{dt} = k_a[N][Cell_A] - k_d \cdot \left(\frac{1}{1 + \left(\frac{[N]}{[N]_{sp}} \right)^{sen}} \right) \cdot [Cell_A] + k_b \cdot \left(1 - \frac{1}{1 + \left(\frac{[N]}{[N]_{sp}} \right)^{sen}} \right) \cdot [Cell_D] \quad [1]$$

$$\frac{d[Cell_D]}{dt} = k_d \cdot \left(\frac{1}{1 + \left(\frac{[N]}{[N]_{sp}} \right)^{sen}} \right) \cdot [Cell_A] - k_b \cdot \left(1 - \frac{1}{1 + \left(\frac{[N]}{[N]_{sp}} \right)^{sen}} \right) \cdot [Cell_D] \quad [2]$$

$$\frac{d[O_2]}{dt} = k_o \cdot (1256 - [O_2]) - k_m[Cell_A][O_2] \quad [3]$$

$$\frac{d[N]}{dt} = -k_a[N][Cell_A] \quad [4]$$

Reg-N functions (32) were used to regulate the rate at which metabolically active cells became dormant and dormant cells became active. Selecting initial parameters was complicated

1
2
3 because the concentration of total cells at each time was unknown, as were the identity and
4 concentration of N . For simplicity, we assigned cell concentration to units of OD_{600} , such that the
5 initial cell concentration was taken as 0.01 (the OD_{600} at the time of inoculation) and the final
6 concentration was taken as 1.4 (OD_{600} at the time of harvesting). Given the assumed
7 stoichiometry that 1 N is required to generate 1 $Cell_A$ (Table 2) and the need for a dramatic
8 decline in $[N]$ to prompt the conversion from $Cell_A \rightarrow Cell_D$, we selected initial $[N]_0 = 1.5$, just
9 greater than the final OD_{600} . This concentration was high enough to generate all of the cells in
10 the experiment but low enough to decline dramatically (percentagewise) during the time-course
11 of the experiment.
12
13
14
15
16
17
18
19
20
21
22
23

24
25 ODEs [1] – [4] were numerically integrated using the NDSolve routine in *Mathematica 9*
26 (<http://www.wolfram.com>). The model was optimized by adjusting parameters k_a , k_b , k_d , k_m , k_o ,
27 $[N]_{sp}$, and sen (Table 2), minimizing the RMSD function defined in Appendix A (Electronic
28 Supplementary Information) to the value 0.016. Simulations (Figure 3, upper panel, solid lines)
29 fit the data acceptably well. The cells used to inoculate the culture were assumed to be dormant
30 ($Cell_D$), so that their conversion to active cells ($Cell_A$) could generate the observed lag phase that
31 preceded exponential growth. Self-replication of active cells and the consumption of O_2 were the
32 most sensitive reactions of the model, whereas the activation of dormant cells was the least
33 sensitive (Table 2). The increase of dormant cells correlated well with the accumulation of large
34 quantities of CW Fe. We conclude that *cells accumulate Fe in their walls as they become*
35 *metabolically inactive.*
36
37
38
39
40
41
42
43
44
45
46
47
48
49
50
51
52

53 **Cell wall iron consists of a heterogeneous distribution of Fe^{III} species.** To characterize CW
54 iron further, we collected MB spectra of Fe-loaded dormant cells at 5, 15, 25, 50, 75, 100, and
55
56
57
58
59
60

1
2
3 150 K (all at 0.05 T parallel-applied magnetic field, Figure 4, A - G) and at perpendicular-
4 applied magnetic fields of 0, 0.75, 1.5, 3, and 6 T (all at 4.2 K, Figure 5). We also collected X-
5 band EPR spectra of such cells at 10, 20, 40 and 80 K (Figure 6, red, yellow, green, and blue
6 lines, respectively). MB spectra were composed of sextet and doublet species, with the sextet
7 representing the majority. Given the results of Figure 1 and Table 1, we presumed that all of the
8 spectral absorption was due to CW Fe, and that the sextet and doublet arose from a paramagnetic
9 $S = 5/2$ Fe^{III} species and a diamagnetic $S = 0$ species, respectively. A small contribution to the
10 sextet intensity was probably due to *vacuolar* mononuclear NHHS Fe^{III} ($S = 5/2$) but this
11 contribution could not be distinguished from the dominating CW Fe^{III}. A small contribution to
12 the doublet intensity was probably due to superparamagnetic Fe^{III} oxyhydroxide nanoparticles.
13 (A portion of the doublet intensity could have arisen from an integer spin species with a very
14 small hyperfine field, but this seems unlikely.) Any central doublet due to mitochondrial
15 [Fe₄S₄]²⁺ clusters and LS Fe^{II} hemes was undetectable due to the dominance of the CW Fe and so
16 we made no attempt to take this feature into account. The high-energy line due to HS Fe^{II} heme,
17 representing a few percent of the overall spectral absorption, was observed at low temperatures,
18 but this was also ignored in fitting.

19
20
21
22
23
24
25
26
27
28
29
30
31
32
33
34
35
36
37
38
39
40
41 At 4.2 K and 0.05 T, diamagnetic and superparamagnetic species could not be
42 distinguished. Collectively they represented ca. 30% of spectral intensity. As the temperature
43 was raised, the *shape* of the spectra changed but the intensity ratio of the sextet to the main
44 doublet remained about the same. This suggested that any superparamagnetic Fe contribution
45 associated with the doublet has a Blocking temperature $T_B \ll 4.2$ K. At high applied fields (e.g.
46 Figure 5E), a superparamagnetic species will magnetically split depending on the hyperfine field,
47 whereas diamagnetic species will not do this. Thus we assigned the ill-resolved region in the
48
49
50
51
52
53
54
55
56
57
58
59
60

1
2
3 middle of the 4.2 K, 6 T spectrum to diamagnetic species. Simulation of this region with an $S = 0$
4
5 Hamiltonian indicated that ca. 20% spectral intensity was due to diamagnetic species. This
6
7 implies that the superparamagnetic species accounts for ca. 10% of spectral intensity. This low
8
9 percentage, along with the broad distribution in hyperfine fields, made it impossible to reliably
10
11 simulate the superparamagnetic species at high field.
12
13
14

15 The sample was transferred from a Mössbauer cup to an EPR tube while maintaining it at
16
17 or near liquid N_2 temperatures. The sample exhibited a $g = 4.3$ EPR signal due to the H.S Fe^{III}
18
19 species. The signal exhibited Curie-Law behavior in that the intensity of the product of signal
20
21 intensity-temperature ($S \cdot T$) was invariant between 10 K and 80 K (Figure 6). The broad $g = 2$
22
23 signal, which we assign to the superparamagnetic species, also seemed to exhibit Curie-Law
24
25 behavior although there was a modest decrease in $S \cdot T$ at low T.
26
27
28

29 Compare the spectroscopic properties of the superparamagnetic nanoparticles to those of
30
31 the 2 - 4 nm diameter nanoparticles in Yah1-depleted mitochondria (30). In Yah1-depleted cells,
32
33 the superparamagnetic doublet had $\delta = 0.52$ mm/s and $\Delta E_Q = 0.62$ mm/s at 5 K; here, $\delta = 0.38$
34
35 mm/s and $\Delta E_Q = 0.50$ mm/s. Like the current superparamagnetic species, Yah1-depleted
36
37 nanoparticles had $T_B \ll 5$ K such that a superparamagnetic doublet was observed at all
38
39 temperatures ≥ 4.2 K. The EPR spectrum associated with nanoparticles from Yah1-depleted
40
41 mitochondria also exhibited a broad $g = 2$ feature with anti-Curie-Law behavior. However, the
42
43 inverse-temperature effect was more dramatic for the nanoparticles of Yah1-depleted
44
45 mitochondria than what we observed here.
46
47
48
49
50
51
52

53 **Kinetics of cell wall iron release by chelation and enzymatic digestion.** The experiments of
54
55 Figure 1 show that CW Fe can be released under different wash conditions. To evaluate the *rate*
56
57
58
59
60

1
2
3 of Fe release, we measured the concentration of cellular Fe as a function of time after treating
4 Fe-loaded cells with water, EDTA at pH 8, or lyticase/EDTA at pH 8. We also monitored the
5 concentration of Fe released into the medium. In all trials, we could account for > 90% of the
6 released Fe. About 80% of CW Fe was removed by treating the cells with lyticase/EDTA for 1 hr
7 (Figure 7, blue lines). The reaction was almost completed in 30 min. Equivalent treatment with
8 EDTA alone (red lines) was less effective whereas treatment with water alone (black lines) was
9 essentially *ineffective*. These results are qualitatively congruent with the MB/EPR experiments
10 described above (however, the MB study suggests that EDTA is less effective in removing CW
11 Fe, compared to EDTA/lyticase treatment, relative to the results of Figure 7). Similar results
12 were obtained using EGTA rather than EDTA (data not shown). We estimate that *over half* of
13 the CW Fe in dormant cells can be removed reasonably well by chelators such as EDTA at pH 8;
14 this estimate assumes that all CW Fe is removed by enzymatic digestion.
15
16
17
18
19
20
21
22
23
24
25
26
27
28
29
30
31
32
33

34 **Metabolically Reactivated Fe-loaded cells grow using Fe mobilized from their internal**
35 **stores AND from Fe in the medium, including trace levels of Fe in Fe-deficient medium.** To
36 evaluate whether cells can utilize their internal Fe stores for growth, we grew cells on $^{57}\text{Fe}_{40}\text{B}_0$
37 medium for 4 days (into stationary phase). After washing 3 times with 100 μM EDTA at pH 7,
38 the resulting metabolically inactive ^{57}Fe -loaded cells contained 4.1 ± 0.4 mM Fe ($n = 3$) (less
39 CW Fe is removed by EDTA at lower pH).
40
41
42
43
44
45
46
47

48 These ^{57}Fe -loaded cells were used to inoculate Fe-deficient Fe_0B_{30} medium, yielding
49 $\text{OD}_{600} \approx 0.01$ at the start of the experiment. The 30 μM concentration of BPS in the medium was
50 > 30 times that required to coordinate all cellular Fe and endogenous Fe in the medium.^{Footnote1}
51
52
53
54
55 The ^{57}Fe -loaded cells in this experiment grew slowly, exhibiting a minimal doubling time (DT)
56
57
58
59
60

1
2
3 of 4.8 hr (Figure 8A, solid circles). In contrast, cells growing on Fe-sufficient minimal medium
4 replicate ~ every 2 hr (24). After 3 - 4 days, the culture that had been inoculated with ^{57}Fe -loaded
5 cells reached a final OD_{600} of 1.6 ± 0.3 ($n = 2$), slightly less than the final $\text{OD}_{600} = 2$ attained by
6 cells grown in standard Fe_{40}B_0 medium. The stationary-state cells contained only $57 \pm 7 \mu\text{M Fe}$
7 ($n = 2$). In contrast, cells on the Fe-sufficient medium and harvested under exponential growth
8 conditions contain 300 - 400 $\mu\text{M Fe}$ (24).
9
10
11
12
13
14
15
16

17 Had the ^{57}Fe -loaded cells *exclusively* used their intracellular stores of ^{57}Fe for growth,
18 and not import any ^{56}Fe from the Fe-deficient medium, they should have doubled 6 times and
19 then stopped growing ($4100 \mu\text{M} \div (2)^6 \approx 57 \mu\text{M}$). The observed OD_{600} change indicates that they
20 actually stopped growing after ~ 7 doublings ($1.6 \div (2)^7 \approx 0.01$). This implies that about half of
21 the Fe used by these cells originated from their ^{57}Fe stores and half from the tiny amount of
22 endogenous ^{56}Fe in the Fe_0B_{30} medium. This result was surprising because yeast cells are
23 commonly thought to be unable to grow on Fe-deficient medium treated with BPS. If the
24 endogenous Fe in BPS-treated medium is chelatable by (and kinetically accessible to) BPS, the
25 tight-binding nature of the $\text{Fe}^{\text{II}}(\text{BPS})_3$ complex implies that virtually all endogenous Fe in the
26 medium should have been chelated by BPS. Perhaps some fraction of the endogenous Fe is
27 inaccessible to BPS yet can be imported and used by cells.
28
29
30
31
32
33
34
35
36
37
38
39
40
41
42
43

44 A second batch of ^{57}Fe -loaded cells with an $[\text{}^{56}\text{Fe}]/[\text{}^{57}\text{Fe}]$ isotope ratio estimated at *ca.* 0.05
45 was transferred to Fe_0B_{30} medium, achieving an initial $\text{OD}_{600} = 0.01$. After 7 doublings the
46 resulting $^{56}\text{Fe}/^{57}\text{Fe}$ ratio in the harvested cells was 1.0 (25 $\mu\text{M } ^{56}\text{Fe}$ and 24 $\mu\text{M } ^{57}\text{Fe}$). The
47 increase in cellular ^{56}Fe must have originated from the trace amounts of ^{56}Fe in the Fe_0B_{30}
48 medium as there was no other source of ^{56}Fe in the experiment. In a third experiment, ^{56}Fe -
49 loaded cells were used to inoculate Fe_0B_{30} medium. In this case, the final $^{56}\text{Fe}/^{57}\text{Fe}$ ratio in the
50
51
52
53
54
55
56
57
58
59
60

1
2
3 harvested cells was 44 ($62 \mu\text{M } ^{56}\text{Fe}$ and $1.4 \mu\text{M } ^{57}\text{Fe}$), again consistent with the import of
4
5 endogenous ^{56}Fe from Fe-deficient media. In both cases, the final $[\text{}^{56}\text{Fe}]/[\text{}^{57}\text{Fe}]$ ratios in the
6
7 harvested cells reflected the relative amounts of the Fe isotopes in the Fe-loaded cells and in the
8
9 endogenous Fe in the medium. We conclude that *Fe-loaded yeast cells can grow on their*
10
11 *internal Fe stores AND on trace amounts of endogenous Fe present in Fe-deficient medium.*
12
13
14
15
16

17 **Metabolically reactivated cells mobilize cell wall Fe^{III} species.** We wanted to identify the type
18
19 of internal Fe stores that are used by Fe-loaded cells to grow on Fe-deficient medium. Our
20
21 approach was to use MB spectroscopy. ^{57}Fe -loaded cells were transferred into 3 different media,
22
23 namely $^{57}\text{Fe}_{40}\text{B}_0$ (the control for which Fe stores should not be used), $\text{Fe}_0\text{B}_{100}$ (Fe-deficient, for
24
25 which Fe stores should be used), and $\text{Fe}_0\text{B}_{100}$ -NAB. The last medium was designed to prevent
26
27 cells from growing in an iron-deficient environment, thereby eliminating the effects of cell
28
29 growth and metabolic activity. In these experiments, the amount of Fe-loaded cells used to
30
31 inoculate fresh media was much greater than in the first set of experiments, such that the OD_{600}
32
33 immediately after inoculation was approximately equal to the OD_{600} when the Fe-loaded cells
34
35 (used for that inoculation) had been previously harvested. This allowed MB spectroscopy (which
36
37 requires large quantities of cells) to monitor changes in cellular Fe content.
38
39
40
41
42

43 The ^{57}Fe -loaded cells initially contained $4.9 \pm 1.5 \text{ mM Fe}$ ($n = 2$). Surprisingly, the cells
44
45 grew equally well on $^{57}\text{Fe}_{40}\text{B}_0$ and $\text{Fe}_0\text{B}_{100}$ media. Thus, cells that were loaded with Fe in their
46
47 CWs and vacuoles grew as fast and to the same final extent in Fe-deficient media as they did in
48
49 Fe-rich media; i.e. the absence of Fe in the medium did not limit the growth rate. The OD_{600} of
50
51 these cultures increased from 1.7 at the time of inoculation to 3.6 after 24 hr of growth (Figure
52
53 8B, solid and open squares, respectively).
54
55
56
57
58
59
60

1
2
3
4
5
6
7
8
9
10
11
12
13
14
15
16
17
18
19
20
21
22
23
24
25
26
27
28
29
30
31
32
33
34
35
36
37
38
39
40
41
42
43
44
45
46
47
48
49
50
51
52
53
54
55
56
57
58
59
60

Despite the same growth rate, the concentration of Fe in the resulting harvested cells was quite different. The cells harvested from the $^{57}\text{Fe}_{40}\text{B}_0$ medium contained 3.9 ± 0.9 mM Fe while those harvested from the $\text{Fe}_0\text{B}_{100}$ medium contained 1.3 ± 0.4 mM Fe ($n = 2$ for each condition). If dilution due to cell growth was the only factor affecting these final cellular Fe concentrations (i.e. if Fe had not been imported from or exported to the environment), the $^{57}\text{Fe}_{40}\text{B}_0$ -grown cells would have contained 2.3 mM Fe after the 24 hr incubation. The fact that they contained more Fe indicates that they (not surprisingly) imported Fe from Fe-rich Fe_{40}B_0 medium. Thus, cells import environmental Fe even if they are not growth-limited by Fe.

The Fe concentration in the cells harvested from $\text{Fe}_0\text{B}_{100}$ medium was 1.8-fold *less* than that expected if they had grown and divided exclusively using their own Fe stores. Where did the rest of their Fe stores go? The simplest interpretation is that the ***Fe-loaded cells mobilized and released ~ 40% of their internal Fe stores when incubated in Fe-deficient medium for 24 hrs.*** We will show below that some of the released Fe coordinated to BPS and that the resulting $\text{Fe}^{\text{II}}(\text{BPS})_3$ complexes adsorbed onto cell surfaces. Counting this absorbed Fe as part of the Fe that was mobilized suggests that these cells actually mobilized much more than 40% of their internal Fe stores during growth after dormancy. Some of the mobilized Fe remained in the growth medium, some coordinated to BPS, and some was reimported into the cell. Only this latter portion supported cell growth. We conclude that ***a large portion of cellular Fe in post-exponential Fe-loaded (dormant) cells is rapidly mobilized when such cells are metabolically reactivated.***

The ^{57}Fe -loaded cells that were transferred into $\text{Fe}_0\text{B}_{100}$ -NAB medium barely grew during the same 24 hr period; the OD_{600} of the culture increased from 1.7 \rightarrow 1.9 (Figure 8B, crosses) whereas the concentration of Fe in these cells declined to 2.9 ± 0.9 mM ($n = 2$). The extent of Fe

1
2
3 loss was greater than could be explained by the effects of growth-associated dilution. Dilution
4 would have caused the Fe concentration to decline only to ~ 4.3 mM. Thus, nearly 30% of the Fe
5
6 in the Fe-loaded cells must have been released and used to support growth after those cells were
7
8 transferred to Fe-deficient medium.
9
10

11
12 We then used MB spectroscopy to investigate the type(s) of Fe centers mobilized by Fe-
13 loaded cells when such cells are grown on Fe-deficient media. The low-temperature low-field
14 MB spectrum of ^{57}Fe -loaded cells (Figure 9A) was dominated by a sextet representing 65% of
15 total spectral intensity. A similar feature is present in the spectra of Figure 1D and 4A which we
16 have shown to be due to CW Fe. This sextet was similar to that arising from vacuolar Fe (33)
17 which is why we previously assigned it as such (24). Another 10% of the spectral intensity was
18 due to a quadrupole doublet in the center of the spectrum (simulated by the blue line in Figure
19 9A). Both features are simulated collectively by the solid red line. The minor differences in
20 simulation parameters relative to those used to fit the spectra of Figures 4 and 5 may reflect
21 batch-to-batch variation as well as uncertainties caused by fitting overlapping spectral features.
22 Some of the intensity of Figure 9A appears to be due to broad, unresolved and poorly
23 characterized magnetic features similar to those described previously (24). MB parameters and
24 total Fe concentrations for these samples are listed in Table S3.
25
26
27
28
29
30
31
32
33
34
35
36
37
38
39
40
41
42

43 The MB spectrum of ^{57}Fe -loaded cells that had grown for 24 hr on $\text{Fe}_0\text{B}_{100}$ medium (Figure
44 9B) was dominated by a narrow quadrupole doublet arising from the $^{57}\text{Fe}^{\text{II}}(\text{BPS})_3$ complex. This
45 doublet, which represented 60% of spectral intensity, was simulated by the dotted line with $\delta =$
46 0.38 mm/s and $\Delta E_Q = 0.30$ mm/s (28). Another 27% of the intensity arose from a NHHS Fe^{III}
47 sextet, and another 10% from NHHS Fe^{II} species (with $\delta = 1.3$ mm/s and $\Delta E_Q = 3.0$ mm/s).
48 These two minor features are highlighted by removing the dominating $\text{Fe}^{\text{II}}(\text{BPS})_3$ doublet
49
50
51
52
53
54
55
56
57
58
59
60

1
2
3 contribution (Figure 9C). The NHHS Fe^{II} doublet is simulated by the green line. The sextet in the
4
5 spectrum of Figure 9C is only ~ 10% as intense as that in the spectrum of Fe-loaded cells
6
7 (consistent with it originating from vacuolar NHHS Fe^{III}). We conclude that ***most (ca. 90%) of***
8
9 ***the Fe^{III} species associated with the CW of Fe-loaded cells was mobilized. Some of this Fe***
10
11 ***helped cells grow on Fe-deficient Fe₀B₁₀₀ medium, some formed a complex with BPS, and***
12
13 ***some remained in solution.***
14
15

16
17 The presence of the ⁵⁷Fe^{II}(BPS)₃ doublet in the spectrum of Figure 9B would be easily
18
19 explained had the cells been grown on BPS medium containing ⁵⁷Fe. BPS is a membrane-
20
21 impermeable Fe^{II} chelator that turns cells pink due to the formation of Fe^{II}(BPS)₃ on the CW
22
23 and/or cell membrane surface (see SI of ref 34). However, the cells used to generate the spectrum
24
25 of Figure 9B were initially loaded with ⁵⁷Fe and then transferred to medium that was essentially
26
27 devoid of Fe (virtually all of the trace endogenous Fe was ⁵⁶Fe). This demonstrates that ***the ⁵⁷Fe***
28
29 ***used to generate the ⁵⁷Fe^{II}(BPS)₃ complex in this sample originated from ⁵⁷Fe that had been***
30
31 ***associated with the CW of ⁵⁷Fe-loaded cells*** that were used to inoculate the Fe₀B₁₀₀ culture. It
32
33 also supports our earlier conclusion that Fe-loaded yeast cells can utilize their CW Fe for growth
34
35 on Fe-deficient medium. Since BPS binds Fe^{II} tightly, these results indicate that ***mobilizing CW***
36
37 ***Fe^{III} species involves reducing it to the Fe^{II} state*** prior to BPS coordination.
38
39
40
41
42
43

44 The Fe-loaded cells that barely grew on Fe₀B₁₀₀-NAB medium exhibited a MB spectrum
45
46 (Figure 9D) that was similar to that of Fe-loaded cells that had been transferred to Fe₀B₁₀₀
47
48 medium and harvested after 24 hr. Major spectral components were due to Fe^{II}(BPS)₃ (48%),
49
50 NHHS Fe^{III} (24%), and two NHHS Fe^{II} species ($\delta = 1.3$ mm/s, $\Delta E_Q = 3.0$ mm/s, 10%; $\delta = 1.1$
51
52 mm/s and $\Delta E_Q = 3.8$ mm/s, 16%; green and maroon lines, respectively, in Figure 9E). The latter
53
54 two doublets arise from a lack of adenine in the medium (35). Under adenine-deficient
55
56
57
58
59
60

1
2
3 conditions, ADE2 mutant strains such as the one used in this study turn pink and accumulate two
4 types of NHHS Fe^{II} species called Fe^{II}_{ON} and Fe^{II}_{ONS}. Since adenine was not supplemented in the
5 Fe₀B₁₀₀-NAB medium, the spectra of these cells included these doublets.
6
7

8
9
10 MB spectra of Fe-loaded cells that had been incubated for 24 hr in Fe-deficient medium
11 were dominated by the Fe^{II}(BPS)₃ doublet. We suspect that this complex was adsorbed on the
12 CW. Waste solutions obtained by washing such cells 3 times with EDTA-containing water and
13 then 3 times in DW were pink due to the leaching of Fe^{II}(BPS)₃ complex from the CW. We
14 calculate that 30% – 40% of the CW Fe was washed away by these rinses. Additional washings
15 were progressively less effective. The Fe^{II}(BPS)₃ doublet observed in MB spectra arose from
16 Fe^{II}(BPS)₃ complexes that remained on the CW after such washings.
17
18
19
20
21
22
23
24
25
26
27
28

29 ***Iron-starved cells can extract endogenous iron from Fe-deficient growth medium but their***
30 ***growth rate and extent of growth is diminished.*** Iron-starved cells should not grow as well on
31 Fe-deficient medium as Fe-loaded cells since they lack Fe stores. To test this idea, Fe-starved
32 cells were inoculated into ⁵⁷Fe₁B₂₁ medium, which is essentially Fe-deficient medium but
33 supplemented with a small amount of ⁵⁷Fe. The cells grew for 15 hr, achieving an OD₆₀₀ ≈ 1.0.
34 They contained 130 ± 20 μM ⁵⁷Fe (n = 2) upon harvesting. Although this was a moderate
35 concentration of Fe, these cells were still “Fe-starved” relative to Fe-loaded cells which contain
36 ≥ 4 mM Fe. Similar Fe concentrations have been observed previously in Fe-starved cells (23). In
37 the previous study, MB spectroscopy revealed that the Fe in these cells was mainly in the form of
38 mitochondrial Fe-S clusters and heme centers, with some NHHS Fe^{II} ions present but no
39 vacuolar NHHS Fe^{III} species. This makes sense because vacuolar Fe^{III} is a storage form of Fe
40 that is not essential for cell metabolism.
41
42
43
44
45
46
47
48
49
50
51
52
53
54
55
56
57
58
59
60

1
2
3 The Fe-starved cells were transferred to Fe₀B₃₀ medium such that OD₆₀₀ was ≈ 0.01
4 immediately after inoculation. They grew to a final OD₆₀₀ of 0.8 ± 0.4 (Figure 8A, open circles)
5 at which point they contained just 23 ± 2 μM Fe (Table S2) (n = 2), ***the lowest cellular Fe***
6 ***concentrations reported for *S. cerevisiae****. Since Fe-starved cells do not store Fe, these cells did
7 not grow quickly or extensively under Fe-deficient conditions. Their minimal DT (5.7 hours)
8 was longer than that of the Fe-loaded cells, and their ultimate cell density was *half* of that
9 attained by Fe-loaded cells. The change of OD₆₀₀ indicated that the Fe-starved cells doubled ~ 6
10 times after they were inoculated into Fe₀B₃₀, whereas the change of cellular Fe implied that the
11 little Fe initially contained in these cells would only allow ~ 2.5 doublings. The Fe required for
12 the additional ~ 3.5 doublings must have originated from the trace endogenous ⁵⁶Fe in the Fe₀B₃₀
13 medium. In support of this, the ⁵⁶Fe/⁵⁷Fe ratio in ⁵⁷Fe-starved cells was 0.3 before inoculation
14 and 4.4 after harvesting. This increase indicates that the cells imported much of their ⁵⁶Fe from
15 the Fe₀B₃₀ medium (virtually all of the endogenous Fe in that medium was ⁵⁶Fe). Each growth
16 and division cycle appears to have been associated with the input of ~ 20 μM ⁵⁶Fe and ~ 3 μM
17 ⁵⁷Fe (Appendix B, Electronic Supplementary Information). This experiment again demonstrates
18 that ***yeast cells can grow using the tiny amount of Fe present in Fe-deficient BPS-treated***
19 ***medium.***

20
21
22
23
24
25
26
27
28
29
30
31
32
33
34
35
36
37
38
39
40
41
42
43
44
45
46 ***Effect of high concentrations of BPS on the growth of Fe-starved and Fe-loaded cells.*** To
47 examine the effect of higher concentrations of BPS on cell growth, we prepared Fe-loaded and
48 Fe-starved cells, and then transferred them to Fe₀B₁₀₀ medium which contained 100 μM rather
49 than 30 μM BPS. (We also standardized the incubation time to 5 days for both Fe-loaded and Fe-
50 starved cells.) The Fe-starved cells barely grew on Fe₀B₁₀₀ (minimal DT = 21 hours), attaining a
51
52
53
54
55
56
57
58
59
60

1
2
3 final OD₆₀₀ of only 0.05 ± 0.02 (Figure 8A, open triangles). The extent of growth implied just 2
4
5 doubling. Fe-starved cells that contained $130 \pm 30 \mu\text{M}$ Fe at the time of transfer to Fe₀B₁₀₀
6
7 should have contained just $\sim 30 \mu\text{M}$ Fe after 2 doublings *if* they exclusively used their own Fe
8
9 for growth. This estimate (we did not measure this concentration) is reasonable because it is
10
11 similar to the minimum cellular Fe concentration of *S. cerevisiae* reported above.
12
13
14

15 The Fe-loaded cells grew on Fe₀B₁₀₀ medium with a minimal DT (5.1 hours) similar to that
16
17 of cells grown on Fe₀B₃₀ medium. However, the final OD₆₀₀ of the culture was only 0.79 ± 0.15
18
19 (Figure 8A, filled triangles), about half of that attained when Fe-loaded cells were grown on
20
21 Fe₀B₃₀ (Figure 8A, filled circles). Cells that began as Fe-loaded at the time of inoculation
22
23 contained $110 \pm 10 \mu\text{M}$ Fe after growing 5 days on Fe₀B₁₀₀ medium. This is approximately *twice*
24
25 the Fe concentration of equivalent cells that were transferred to Fe₀B₃₀ medium and grown to
26
27 approximately the same stage.
28
29
30

31 Thus, cells grown on a more extreme Fe-deficient medium grew to half the culture density
32
33 and contained twice as much Fe as cells grown on less extreme Fe-deficient medium. Why? One
34
35 could argue that they ran out of endogenous Fe sooner because there was less of it - but if that
36
37 were the case why didn't they grow on their internal Fe stores?
38
39
40

41 We hypothesize that the *CW iron in Fe-loaded cells is in a form that cannot support*
42
43 *growth directly; it must first be mobilized and released into the environment before it can be*
44
45 *reimported and used by the cell.* Accordingly, BPS short-circuits this mobilization process by
46
47 intercepting the mobilized Fe before it can be reimported into the cell, with higher concentrations
48
49 of BPS in the medium more effective in doing this than lower concentrations. We further
50
51 hypothesize that this Fe mobilization-reimport process requires metabolic energy, and that the
52
53 cells stopped growing because they lacked the energy needed to drive mobilization. Thus, once
54
55
56
57
58
59
60

1
2
3 CW Fe^{III} is reduced, the Fe^{II} becomes available for coordination to BPS for import into the
4
5 cytosol. BPS at a higher concentration will react faster with mobilized Fe^{II}, forming more
6
7 Fe^{II}(BPS)₃ which can no longer be reimported into the cytosol or used in metabolism. The
8
9 metabolic activity of the Fe-starved cells gradually declines, preventing further growth.
10
11

12
13
14 ***Mobilized cell wall iron dissociates into the growth medium.*** To further assess whether
15
16 mobilized CW Fe dissociates from the cell and moves into the growth medium, we directly
17
18 measured Fe in three MM-based media (Fe₀B₁₀₀, Fe₀B₀, and ⁵⁶Fe₄₀B₀) after each had been
19
20 inoculated with ⁵⁷Fe-loaded cells. The first two media lacked added Fe; their endogenous ⁵⁶Fe
21
22 and ⁵⁷Fe concentrations were measured to be 230 nM and 8 nM, respectively. The third medium
23
24 contained 40 μM of added ⁵⁶Fe. We used DW as a fourth medium, which contained 43 nM ⁵⁶Fe
25
26 and 2 nM ⁵⁷Fe prior to inoculation. ⁵⁷Fe-loaded cells were inoculated into each medium to about
27
28 the same cell density as when they had been harvested. OD₆₀₀ was then monitored for 24 hr, and
29
30 then cells were harvested and analyzed by ICP-MS and MB spectroscopy. The concentration of
31
32 Fe in the media itself was measured at different times during the incubations to obtain direct
33
34 evidence that Fe dissociates from cells.
35
36
37
38
39

40
41 Cells in the first three media grew at similar rates and extents (Figure 8C, open squares,
42
43 solid diamonds and solid squares, respectively), relative to each other and to cells grown in
44
45 standard ⁵⁷Fe₄₀B₀ medium (Figure 8B, solid squares). In the experiment of Figure 8C, OD₆₀₀
46
47 increased regardless of media ($n = 2$ for ⁵⁷Fe₄₀B₀; $n = 3$ for Fe₀B₁₀₀ and $n = 3$ for Fe₀B₀). This
48
49 indicated *one* cell doubling. The concentration of Fe in the Fe-loaded cells that were incubated in
50
51 Fe₀B₁₀₀ declined from 3.9 ± 0.7 mM before inoculation to 1.5 ± 0.2 mM thereafter (Table S2),
52
53 similar to our previous results. There was a similar decline (to 1.2 ± 0.2 mM) in the Fe
54
55
56
57
58
59
60

1
2
3 concentration of the cells incubated in Fe₀B₀. At face-value, these results suggest that the ⁵⁷Fe-
4 loaded cells that were incubated in Fe₀B₁₀₀ and Fe₀B₀ media respectively mobilized about 23%
5 and 40% of their CW Fe into the media during the 24 hr period when they doubled. Cells
6 actually mobilized more Fe because the ⁵⁷Fe^{II}(BPS)₃ that adhered to the CW (and was included
7 in the measured cellular [Fe]) originated from Fe^{II} that had also been mobilized.
8
9

10
11 The Fe concentration of ⁵⁷Fe-loaded cells after growth on ⁵⁶Fe₄₀B₀ medium was 3.1 mM
12 (Table S2, Figure 8C, solid squares), 21% lower than at the time of inoculation. However, since
13 the OD₆₀₀ doubled, the total amount of Fe in the entire population of cells must have increased
14 by ~ 52% while the ⁵⁷Fe portion decreased by ~ 57%. This indicates that CW ⁵⁷Fe was mobilized
15 and released as ⁵⁶Fe was simultaneously imported. Hence, ***even under Fe-sufficient conditions,***
16 ***metabolically active cells mobilize and import CW Fe while they simultaneously reduce and***
17 ***import environmental Fe.***
18
19
20
21
22
23
24
25
26
27
28
29
30
31

32 Metabolically *inactive* cells placed in DW also lost Fe. The Fe concentration of ⁵⁷Fe-
33 loaded cells placed in DW for 24 hr decreased by 46% ($\{^{Fe}3.9 \times OD2.2 - Fe2.1 \times OD2.2\} \div \{^{Fe}3.9$
34 $\times OD2.2\}$) even though the cells barely grew (Figure 8C, open diamonds). We regard this as Fe
35 *leaching* from the CW rather than metabolic mobilization.
36
37
38
39
40

41 Loss of cellular Fe was confirmed by measuring the Fe concentration in media to which
42 cells had been incubated. ⁵⁷Fe concentrations in Fe₀B₁₀₀, Fe₀B₀, and DW media at different times
43 after ⁵⁷Fe-loaded cells were inoculated are shown in Figure 10A. Prior to incubation, the residual
44 total Fe concentration in Fe₀B₁₀₀ and Fe₀B₀ media was 0.24 μM (0.008 μM ⁵⁷Fe) while that in
45 DW was 0.045 μM (0.002 μM ⁵⁷Fe). The OD₆₀₀ was 2.1 immediately after ⁵⁷Fe-loaded cells
46 were added. At different times, cells were removed by centrifugation and the Fe concentration in
47 the medium was measured. Within 15 min of inoculation, the ⁵⁷Fe concentration in Fe₀B₁₀₀
48
49
50
51
52
53
54
55
56
57
58
59
60

1
2
3 medium increased to 2 μM (Figure 10A, solid squares). Then the ^{57}Fe concentration decreased,
4 reaching 0.4 μM at 24 hr. The concentration of ^{56}Fe in the medium dropped 0.12 μM over the
5 first 12 hr (Figure 10B, open diamonds). A UV-vis spectrum of ^{57}Fe -loaded cells that had been
6 incubated for 24 hr in $\text{Fe}_0\text{B}_{100}$ medium showed strong absorption at 535 nm (Figure S1, B vs. A)
7 that reflected $\text{Fe}^{\text{II}}(\text{BPS})_3$ complexes associated with these unwashed cells. A corresponding MB
8 spectrum revealed that > 90% of Fe associated with these cells was $^{57}\text{Fe}^{\text{II}}(\text{BPS})_3$ (Figure 11D).
9 Much of that $^{57}\text{Fe}^{\text{II}}(\text{BPS})_3$ complex was removed by washing at high pH (see below, Figure S1, C
10 and D and Figure 11E). We conclude that *much of the CW Fe in Fe-loaded cells was mobilized*
11 *and released into the Fe-deficient medium after which a significant portion bound BPS and*
12 *adsorbed on the CW.*

13
14
15
16
17
18
19
20
21
22
23
24
25
26
27
28
29
30
31
32
33
34
35
36
37
38
39
40
41
42
43
44
45
46
47
48
49
50
51
52
53
54
55
56
57
58
59
60
Whether the mobilized Fe^{II} ions were “cleanly” released from the CW and then coordinated by BPS and re-adsorbed onto the CW, or whether BPS coordinated Fe^{II} ions that remained *loosely* associated with the CW, is unknown. However, at least some of the mobilized Fe was released into the medium as evidenced by direct measurement. The kinetics of this experiment suggest an initial fast mobilization-and-release phase was followed by a slow-release phase that occurred as Fe was reimported into the cells.

For the experiment involving Fe_0B_0 medium, the concentration of ^{57}Fe in the medium increased to $\sim 2 \mu\text{M}$ immediately after incubation (Figure 10A, solid triangles), similar to the experiment involving $\text{Fe}_0\text{B}_{100}$ medium, but it then remained nearly invariant for 24 hr rather than decline. Why the difference? Fe_0B_0 medium lacks BPS, and so in this medium the exported ^{57}Fe stayed in solution rather than re-associate with the CW. Fe_0B_0 -grown cells contained 1.2 mM Fe while $\text{Fe}_0\text{B}_{100}$ -grown cells contained 1.5 mM Fe due to this association of $\text{Fe}^{\text{II}}(\text{BPS})_3$ with the CW. The 1.5 mM value might underestimate the magnitude of this effect because some

1
2
3 Fe^{II}(BPS)₃ complexes were removed from the CW during rinsing. In the absence of BPS, the
4 mobilized ⁵⁷Fe ions must have been imported into the cytosol where they were used to support
5 cell growth. The rates of these two processes (CW Fe mobilization and release vs. Fe import into
6 the cytosol) appear to be similar since the concentration of Fe in the medium was largely
7 invariant for 24 hr.
8
9

10
11
12
13
14
15 The low-temperature low-field MB spectrum of the corresponding cells after 24 hr
16 incubation (Figure 11B) was dominated by an Fe^{III} sextet along with significant intensity of the
17 central quadrupole doublet that is primarily due to mitochondrial respiratory complexes (green
18 line). The MB spectrum of the original ⁵⁷Fe-loaded cells used in this experiment (Figure 11A)
19 exhibited an intense sextet and doublet, features which were strongly diminished in spectra of the
20 post-incubation cells. This indicates that ⁵⁷Fe-loaded cells exported nearly all of their CW Fe^{III}.
21
22 Some mobilized CW Fe was likely used to synthesize the Fe/S clusters and heme centers giving
23 rise to the central doublet in Figure 11B.
24
25
26
27
28
29
30
31
32
33

34 Interpreting the effect of incubating Fe-loaded cells in DW proved to be difficult despite
35 the absence of any cell-growth effects. Consistent with the decrease in cellular Fe, the ⁵⁷Fe
36 concentration in DW increased gradually (Figure 10A, open circles), indicating that ⁵⁷Fe had
37 exited the cells that had been placed in water. Consistent with that, the intensity of the
38 corresponding MB spectrum declined (Figure 11C) to about half of that observed for Fe-loaded
39 cells (Figure 11A). Curiously, the components in that spectrum and their relative percentages,
40 before and after incubation in water, were nearly identical. Viewed naively, this would imply
41 that all Fe in the metabolically inactive cells (not just CW Fe) was slowly released in proportion
42 to the amount present. We conclude that *metabolically inactive cells “leach” CW Fe but they do*
43
44
45
46
47
48
49
50
51
52
53
54
55
56
57
58
59
60 *not mobilize it* in contrast to metabolically reactivating cells.

1
2
3 The overall concentration of Fe in the cells incubated in $^{56}\text{Fe}_{40}\text{B}_0$ decreased $\sim 20\%$ after 24
4 hr of incubation (3.9 mM \rightarrow 3.1 mM) during which time the cells underwent a single doubling.
5
6 The $^{56}\text{Fe}/^{57}\text{Fe}$ ratio changed from 0.03 to 2.6, indicating both mobilization and release of ^{57}Fe
7
8 from the CW AND the import of ^{56}Fe from the medium. Initially, $[^{56}\text{Fe}]_1 = 0.1$ mM and $[^{57}\text{Fe}]_1 =$
9
10 3.8 mM (the subscript indicates the generation number) whereas after doubling, $[^{56}\text{Fe}]_2 = 2.2$
11
12 mM and $[^{57}\text{Fe}]_2 = 0.9$ mM. Thus in one doubling the cells increased $[^{56}\text{Fe}]$ by 2.1 mM and
13
14 decreased $[^{57}\text{Fe}]$ by 2.9 mM. This may seem like an extremely rapid rate of exchange, but the
15
16 time required for that doubling event was far longer than takes place under standard exponential
17
18 growth conditions (24 hr. vs. 2 hr.).
19
20
21
22
23

24 The overall concentration of Fe in the $^{56}\text{Fe}_{40}\text{B}_0$ medium declined during the 24 hr
25 incubation (Figure 10B, solid circles), consistent with the import of ^{56}Fe into the cell and with
26
27 the doubling of cellular content. In $^{56}\text{Fe}_{40}\text{B}_0$ medium, the concentration of ^{56}Fe (open diamonds)
28
29 declined while that of ^{57}Fe (solid diamonds) increased during the initial 15 min, again consistent
30
31 with the import of ^{56}Fe into the cell and the rapid loss of ^{57}Fe . The total Fe concentration in the
32
33 medium was invariant during this period, indicating that cellular and environmental Fe ions
34
35 exchange at roughly equal rates.
36
37
38
39

40 The MB spectrum of the ^{57}Fe -enriched cells that had been incubated for 24 hr in $^{56}\text{Fe}_{40}\text{B}_0$
41 medium (Figure 11F) displayed just the ^{57}Fe ions that were retained in the cells (imported ^{56}Fe
42
43 was MB-invisible and any released ^{57}Fe was no longer associated with the cells). Consistent with
44
45 a decrease in ^{57}Fe concentration (5.2 \rightarrow 0.7 mM; Table S2), there was approximately a 5-fold
46
47 decline in overall spectral intensity. Much of the lost Fe appears to have been CW Fe^{III} species.
48
49 The spectrum displayed an increase in the NHHS Fe^{II} doublet (Figure 11F, orange line) which
50
51 may represent the reduced form of the mobilized CW Fe^{III} species.
52
53
54
55
56
57
58
59
60

1
2
3
4
5
6 *Fe^{II}(BPS)₃ desorption from the cell wall depends on pH.* BPS is a negatively-charged chelator
7
8 that should be unable to penetrate neutral or negatively charged cell membranes. This property is
9
10 probably due to the large size of the molecule and to charge-charge repulsion involving
11
12 negatively charged groups on the yeast CW (4). So why does [Fe^{II}(BPS)₃]⁴⁻ adhere to the CW?
13
14 We hypothesize that it is actually neutral or positively charged at the pH of the medium, which
15
16 would facilitate CW binding via hydrophobic or electrostatic interactions. The pH of Fe₄₀B₀
17
18 medium dropped from 4.6 to 3.1 during the 24 hr experiments. The pKa of the sulfonic acid
19
20 groups on Fe^{II}(BPS)₃ are 2.83 and 5.20 (36) which implies that a portion of the Fe^{II}(BPS)₃
21
22 molecules should be neutral at the pH of the experiment.
23
24
25
26

27
28 Given these considerations, we endeavored to remove Fe^{II}(BPS)₃ from the CW by rinsing
29
30 the pink cells with chilled 100 mM Tris at pH 9.4. At this pH, the complex should be negatively
31
32 charged and, if our hypothesis is correct, no longer attracted to the CW or plasma membrane.
33
34 Upon adding the high-pH buffer, the cells turned off-white and the washes turned an intense
35
36 pink, indicating the large-scale release of the Fe^{II}(BPS)₃ complex into the buffer (Figure S1, D).
37
38 UV-vis spectra of the pink and off-white cells confirmed that Fe^{II}(BPS)₃ had been removed
39
40 (Figure S1, C vs. B). MB spectra of the equivalent cells showed that most of the Fe^{II}(BPS)₃
41
42 complex was gone; the remaining Fe exhibited features commonly associated with normal yeast
43
44 cells, such as the central doublet and HS Fe^{II/III} features. However, these features were present at
45
46 low levels (Figure 11 E vs. D, Table S2).
47
48
49
50
51
52

53 *Nonheme high-spin Fe^{II} forms transiently during initial stages of cell wall iron mobilization.*

54
55 To investigate the kinetics and mechanism of Fe mobilization from ⁵⁷Fe-loaded cells after being
56
57
58
59
60

1
2
3 transferred into $\text{Fe}_0\text{B}_{100}$ medium, we collected MB spectra of these cells 0, 0.5, 3 and 6 hr after
4
5 transferring them into $\text{Fe}_0\text{B}_{100}$ medium. The 0.5 hr spectrum (Figure 12B) exhibited features
6
7 similar to those of original ^{57}Fe -loaded cells (Figure 12A), except that the NHHS Fe^{II} doublet
8
9 was three-times more intense (see arrow in Figure 12B; Table S3). At that time, the $\text{Fe}^{\text{II}}(\text{BPS})_3$
10
11 doublet had barely begun to form (Figure 12B, pink line). At longer times, NHHS Fe^{II} and
12
13 diamagnetic/superparamagnetic Fe^{III} features diminished as the intensity of the $\text{Fe}^{\text{II}}(\text{BPS})_3$
14
15 doublet increased (Figures 12C and S2). The NHHS Fe^{III} sextet also decreased, perhaps with a
16
17 slight delay relative to the other processes (Figure S2, open squares vs. solid circles and squares).
18
19 The $\text{Fe}^{\text{II}}(\text{BPS})_3$ doublet had reached $\sim 50\%$ of the total intensity by 6 hr (Figure 12D), eventually
20
21 climbing to $\sim 90\%$ by 24 hr (Figure S2, solid circles). These results demonstrate that *an early*
22
23 *step in CW Fe mobilization is the formation of NHHS Fe^{II} from Fe^{III} CW species, followed by*
24
25 *BPS coordination.*
26
27
28
29
30
31
32
33

34 ***The Iron Regulon is not expressed during the accumulation of cell wall iron.*** We examined the
35
36 level of Fet3p expression in various media and at different times. In cells grown on $\text{Fe}_0\text{B}_{100}$,
37
38 Fet3p was expressed at all times (Figure 13, bottom panel). However, maximal expression was at
39
40 12 hr when the cells were growing exponentially (see Figure 8C). As cells entered stationary
41
42 state, Fet3p expression declined to an extent similar to that observed previously (24). This is
43
44 consistent with the decreased need for Fe under stationary growth conditions. In the absence of
45
46 BPS, Fet3p expression was reduced. In $^{56}\text{Fe}_{40}\text{B}_0$ medium, cells did not express much Fet3p
47
48 because Fe was abundant in the medium. In *DW*, cells did not express Fet3p because they were
49
50 metabolically inactive. These measurements suggest that *the Aft1/2-dependent iron regulon is*
51
52 *not expressed under post-exponential conditions when the cell becomes dormant and Fe*
53
54
55
56
57
58
59
60

1
2
3 *accumulates in the CW*. Iron regulon proteins probably promote CW Fe mobilization via the
4
5 reductive Fe uptake system.
6
7
8
9

10 **Conclusions**

11
12 The major conclusions of this study are summarized in the model of Figure 14. Iron
13
14 accumulates in the walls of yeast cells that are declining in metabolic activity (transitioning from
15
16 exponential to post-exponential growth stages). This phenomenon is probably prompted by the
17
18 lack of certain metabolites (possibly glucose) within the cell. Metal ion accumulation appears
19
20 specific for Fe in that Cu, Mn, and Zn do not accumulate in the CW. In metabolically dormant
21
22 cells, CW Fe accounts for ~ 90% of total cellular Fe; thus, the accumulation of CW Fe represents
23
24 a *huge* perturbation of the Fe content of a yeast cell.
25
26
27

28
29 Our results show that the majority of CW Fe (~70%) is present as mononuclear NHHS
30
31 Fe^{III} ions, with modest levels of diamagnetic Fe species (~ 20%) and even less
32
33 superparamagnetic Fe^{III} oxyhydroxide nanoparticles (~10%). It is tempting to speculate that Fe
34
35 initially accumulates as magnetically isolated mononuclear Fe^{III} species, then as Fe accumulates
36
37 to a higher density, magnetic interactions develop that give rise to the diamagnetic and finally
38
39 superparamagnetic species. The CW contains a large number of negatively charged
40
41 phosphodiester bridges in both N- and O-carbohydrate side chains that anchor the protein to the
42
43 CW (37). Fe coordinates other phosphodiester species (38) suggesting this mode of binding. Fe^{III}
44
45 may bind to various sites in the CW (39). Bound Fe may also serve to stabilize the CW structure.
46
47
48
49

50
51 When dormant cells reactivate, CW Fe^{III} species become mobilized regardless of the Fe
52
53 concentration in the growth medium. Mobilization involves reduction to the Fe^{II} state probably
54
55 via a reaction catalyzed by surface ferric reductases (40). CW Fe may dissociate even when not
56
57
58
59
60

1
2
3 reduced to Fe^{II}, but this is a different phenomenon that we call *leaching*. The reducing
4
5 equivalents used for mobilization must originate from the metabolic activity of the cell (41).
6
7 Mobilized Fe^{II} is released from the CW; some is imported into the cytosol for cell growth and
8
9 some remains in the environment. Thus, CW Fe becomes available as dormant cells awaken. If
10
11 chelators such as BPS or EDTA are present in the environment, they will also coordinate
12
13 mobilized Fe^{II}. Metabolically active cells can also import trace amounts of endogenous forms of
14
15 Fe in Fe-deficient (BPS-treated) growth media. The cell does not discriminate strongly in its
16
17 source of imported Fe - it simultaneously imports mobilized CW Fe AND endogenous Fe from
18
19 the medium. Given the scarcity of bioavailable Fe in the environment, the CW Fe accumulation-
20
21 mobilization-re-importation process would have provided a selective advantage during evolution.
22
23
24
25
26

27 Our results demonstrate that the CW should be regarded as a second storage compartment
28
29 for Fe in *S. cerevisiae* and probably in other fungal cells. Its function in this regard is distinct
30
31 from that of vacuoles; vacuolar Fe maintains intracellular homeostasis which allows
32
33 metabolically active cells to survive in Fe-poor environments and it also sequesters potentially
34
35 toxic forms of Fe. CW Fe helps reactivate dormant cells, by providing Fe regardless of the
36
37 availability of Fe in the environment. Given the large extent of Fe accumulation, the CW should
38
39 be regarded, along with mitochondria and vacuoles, as a major iron traffic “hub” in yeast.
40
41
42

43 During exponential growth, the reductive Fe uptake system controlled by the Aft1/2-
44
45 dependent iron regulon may reduce bound Fe^{III} such that the Fe could be imported and not
46
47 accumulate in the CW. After the cell enters post-exponential growth, the iron regulon is shut
48
49 down and CW bound Fe cannot be reductively mobilized; thus it accumulates. The Fit genes are
50
51 part of the iron regulon, and so their expression should also decline. If the Fit proteins facilitate
52
53 passage of Fe across the CW and into the cytosol, we would expect that Fe should accumulate
54
55
56
57
58
59
60

1
2
3 during post-exponential growth, as is observed. Conflicting with this expectation is the observed
4
5 *decline* in CW Fe in mutant strains lacking Fit proteins (17). Further studies are needed to
6
7 reconcile this situation.
8
9

10 One practical ramification of our study is that researchers who measure Fe concentrations
11
12 of whole fungal cells should not grow cells beyond exponential phase, because the dominating
13
14 contribution of CW Fe to the total cellular Fe could cause confusion. One should also be cautious
15
16 in using BPS to generate Fe-deficient conditions. Doing so creates an Fe deficiency severe
17
18 enough to turn-on the iron regulon (42, 43) but not severe enough to fully abolish growth.
19
20 Amazingly, yeast cells can import trace endogenous Fe from such media and use it for growth.
21
22
23

24 Other fungal cells besides *S. cerevisiae* have CWs, and some connections with iron
25
26 metabolism have been reported. Vainshtein *et al.* identified Fe nanoparticles in the CW of the
27
28 pathogenic fungus *Cryptococcus humicola* (16). Cir1, the “master iron regulator” in the pathogen
29
30 *Cryptococcus neoformans*, regulates CW biogenesis and other virulence factors (44). The
31
32 polysaccharide capsule of these cells is a major virulence factor, and capsule production is
33
34 enhanced under Fe-limiting conditions (8). In *Candida glabrata*, CW proteins CgCcw14 and
35
36 CgMam3 are “pivotal virulence determinants” that are involved in iron metabolism (45).
37
38 CgCcw14 is a cysteine-rich glycosylphosphatidylinositol-linked CW protein while CgMam3 is a
39
40 putative hemolysin. Ferric reductase Cfl1 in *Candida albicans* is involved in CW integrity,
41
42 morphogenesis, virulence and invasion into host cells (10). Mutant cells lacking Cfl1 overload
43
44 with Fe, but whether the Fe accumulates in the CW or elsewhere was not investigated (11). We
45
46 suspect that the CW Fe accumulation phenomenon discovered here is a general property of
47
48 fungi, and that it promotes their survival. If so, inhibiting CW Fe may diminish the ability of
49
50 pathogenic fungi to survive in a host (7). Deleting the Fet3 ferroxidases on the plasma membrane
51
52
53
54
55
56
57
58
59
60

1
2
3 of pathogenic fungus *Colletotrichum graminicola* caused an 80% decline in chitin synthase and
4 defects in the CW that reduced virulence. These proteins are part of the reductive iron import
5 system which is required for CW integrity/stability and pathogenic fungal virulence; indeed the
6 ability to import Fe is considered a “key factor for pathogenicity”. Future studies should
7 investigate whether pathogenicity is related to the ability of the CW to accumulate and/or
8 mobilize Fe as such investigations may lead to improved treatments for fungal pathologies.
9
10
11
12
13
14
15
16
17
18
19

20 Acknowledgements

21
22 We thank Brad Pierce (University of Texas at Arlington) for kindly allowing us to use his
23 EPR spectrometer, Andrew Dancis (University of Pennsylvania) for generously providing the
24 Fet3 antibody, and Charles Johnson (University of Tennessee) for help in analyzing Mössbauer
25 spectra. The National Institutes of Health (GM084266) and the Robert A. Welch Foundation
26 (A1170) sponsored this study.
27
28
29
30
31
32
33
34
35
36

37 Footnotes

38
39 **Footnote 1:** If all of the ^{57}Fe in these cells were released into the medium, the final ^{57}Fe
40 concentration in the medium would have been ~ 80 nM. At an $\text{OD}_{600} = 1.0$, 250 mL of cell
41 culture packs into a volume of ~ 700 μL , which suggests that cultures with $\text{OD}_{600} = 0.01$ should
42 pack into a volume of ~ 7 μL . Assuming a packing efficiency of 0.7, this corresponds to ~ 5 μL
43 of cells. The concentration of Fe in this volume of 4.1 mM Fe, if diluted into 250 mL, would be
44 ~ 80 nM. The endogenous concentration of ^{56}Fe in Fe_0B_0 medium was 0.3 ± 0.2 μM ($n = 3$).
45
46
47
48
49
50
51
52
53
54

55 References

- 1
2
3 1. G. Lesage, and H. Bussey, Cell wall assembly in *Saccharomyces cerevisiae*, *Microbiol*
4 *and Mol. Biol. Rev.* 2006, **70**, 317-343.
- 5
6
7 2. J.G. De Nobel, F.M. Klis, J. Priem, T. Munnik, and H. VanDenEnde, The gluconase-
8 soluble mannoproteins limit cell wall porosity in *Saccharomyces cerevisiae*, *Yeast*, 1990, **6**, 491-
9 499.
- 10
11
12 3. P.W.J. DeGroot, A.F. Ram, and F.M. Klis, Features and functions of covalently linked
13 proteins in fungal cell walls, *Fungal Genet. Biol.*, 2005, **42**, 657-675.
- 14
15
16 4. F.M. Klis, M. de Jong, S. Brul, and P.W.J. de Groot, Extraction of cell surface-associated
17 proteins from living yeast cells, *Yeast*, 2007, **24**, 253-258.
- 18
19
20 5. P.W.J. DeGroot, C. Ruiz, C.R. Vazquez de Aldana, E. Euienas, V.J. Cid, F. Del Rey, et
21 al. A genomic approach for the identification and classification of genes involved in cell wall
22 formation and its regulation in *Saccharomyces cerevisiae*, *Comp. Funct. Genomics* 2001, **2**, 124-
23 142.
- 24
25
26 6. F.M. Klis, A. Boorsma, and P.W.J. DeGroot, Cell wall construction in *Saccharomyces*
27 *cerevisiae*, *Yeast* 2006, **23**, 185-202.
- 28
29
30 7. E. Albarouki, and H.B. Deising, Infection structure-specific reductive iron assimilation is
31 required for cell wall integrity and full virulence of the maize pathogen *Colletotrichum*
32 *graminicola*, *Mol. Plant-Microbe Interact.* 2013, **26**, 695-708.
- 33
34
35 8. S.E. Vartivarian, E.J. Anaissie, R.E. Cowart, H.A. Sprigg, M.J. Tingler, and E.S.
36 Jacobson, Regulation of cryptococcal capsular polysaccharide by iron, *J. of Infect. Dis.* 1993,
37 **167**, 186-190.

- 1
2
3 9. V.K. Srivastava, K.J. Suneetha, and R. Kaur, A systematic analysis reveals an essential
4 role of high-affinity iron uptake system, haemolysin and CFEM domain-containing protein in
5 iron homoeostasis and virulence in *Candida glabrata*, *Biochem. J.* 2014, **463**, 103-114.
6
7
- 8
9
10 10. Q. Yu, Y. Dong, N. Xu, K. Qian, Y. Chen, B. Zhang, L. Xing, and M. Li, A novel role of
11 the ferric reductase Cfl1 in cell wall integrity, mitochondrial function, and invasion to host cells
12 in *Candida albicans*, *FEMS Yeast Res.* 2014, **14**, 1037-1047.
13
14
- 15
16
17 11. N. Xu, K. Qian, Y. Dong, Y. Chen, Q. Yu, B. Zhang, L. Xing, and M. Li, Novel role of
18 the *Candida albicans* ferric reductase gene CFL1 in iron acquisition, oxidative stress tolerance,
19 morphogenesis and virulence, *Res. Microbiol.* 2014, **165**, 252-261.
20
21
- 22
23
24 12. G.H. Fleet, and H.J. Phaff, Ultrastructure of the Cell-Wall of *Schizosaccharomyces*
25 *pombe* following treatment with various gluconases, *J. Structural Biol.* 1995, **114**, 140-152.
26
27
- 28
29
30 13. E. Cabib, T. Drgon, J. Drgonova, R.A. Ford, and R. Kollar, The yeast cell wall, a
31 dynamic structure engaged in growth and morphogenesis, *Biochem. Soc. Trans.* 1997, **25**, 200-
32 204.
33
34
- 35
36
37 14. R.C. Goldman and A. Branstrom, Targeting cell wall synthesis and assembly in
38 microbes: similarities and contrasts between bacteria and fungi, *Curr. Pharmaceutical Design.*
39 1999, **5**, 473-501.
40
41
- 42
43
44 15. P. Orlean, Biogenesis of yeast wall and surface components In (Pringle JR, Broach JR
45 and Jones E.W., editors) "The molecular and cellular biology of the yeast *Saccharomyces* Vol 3.
46 Cell cycle and cell biology" Cold Spring Harbor Monograph series, 1997, 21, 229-362.
47
48
- 49
50
51 16. M. Vainshtein, N. Belova, T., Kulakovskaya, N. Suzina, and V. Sorokin, Synthesis of
52 magneto-sensitive iron-containing nanoparticle by yeasts, *J. Ind. Microbiol. Biotechnol.* 2014,
53 41, 657-663.
54
55
56
57
58
59
60

- 1
2
3
4
5
6
7
8
9
10
11
12
13
14
15
16
17
18
19
20
21
22
23
24
25
26
27
28
29
30
31
32
33
34
35
36
37
38
39
40
41
42
43
44
45
46
47
48
49
50
51
52
53
54
55
56
57
58
59
60
17. O. Protchenko, T. Ferea, J. Rashford, J. Tiedeman, P.O. Brown, D. Botstein, and C.C. Philpott, Three cell wall mannoproteins facilitate the uptake of iron in *Saccharomyces cerevisiae*, *J. Biol. Chem.* 2001, **276**, 49244-49250.
 18. J.H. Scott and R. Schekman, Lyticase – endoglucanase and protease activities that act together in yeast cell lysis, *J. Bacteriol.* 1980, **142**, 414–423.
 19. K. Chojnacka, Biosorption and bioaccumulation – the prospects for practical applications, *Environment Internatl.* 2010, **36**, 299-307.
 20. C.E. Outten and A.N. Albetel, Iron sensing and regulation in *Saccharomyces cerevisiae*: ironing out the mechanistic details, *Curr. Opin. Microbiol.* 2013, **16**, 662-668.
 21. R. Lill, B. Hoffmann, S. Molik, A.J. Pierik, N. Rietzschei, O. Stehling, M.A. Uzarska, H. Webert, C. Wibrecht, and U. Mühlenhoff, The role of mitochondria in cellular iron-sulfur protein biogenesis and iron metabolism, *Biochim. Biophys. Acta*, 2012, **1823**, 1491-1508.
 22. L. Li, R. Miao, S. Bertram, X. Jia, D.M. Ward, and J. Kaplan, A role for iron-sulfur clusters in the regulation of transcription factor yap5-dependent high iron transcriptional responses in yeast, *J. Biol. Chem.* 2012, **287**, 35709-35721.
 23. G.P. Holmes-Hampton, N.D. Jhurry, S.P. McCormick, and P.A. Lindahl, Iron content of *Saccharomyces cerevisiae* cells grown under iron-deficient and iron-overload conditions, *Biochemistry*, 2013, **52**, 105-114.
 24. J. Park, S.P. McCormick, M. Chakrabarti, and P.A. Lindahl, The lack of synchronization between iron uptake and cell growth leads to iron overload in *Saccharomyces cerevisiae* during post-exponential growth modes, *Biochemistry* 2013, **52**, 9413-9425.

- 1
2
3
4
5
6
7
8
9
10
11
12
13
14
15
16
17
18
19
20
21
22
23
24
25
26
27
28
29
30
31
32
33
34
35
36
37
38
39
40
41
42
43
44
45
46
47
48
49
50
51
52
53
54
55
56
57
58
59
60
25. J. Park, S.P. McCormick, M. Chakrabarti, and P.A. Lindahl, Insights into the iron-ome and manganese-ome of Δ mtm1 *Saccharomyces cerevisiae* mitochondria, *Metalloomics*, 2013, **5**, 656-672.
26. P.A. Lindahl, J.G. Morales, R. Miao, and G.P. Holmes-Hampton, Isolation of *Saccharomyces cerevisiae* Mitochondria for Mössbauer, EPR and Electronic Absorption Spectroscopic Analyses, *Meth. Enzymol.*, 2009, **456**, Ch. 15, 268-286.
27. R. Miao, G.P. Holmes-Hampton, and P.A. Lindahl, Biophysical investigation of the iron in Aft1-1(up) and Gal-Yah1 *Saccharomyces cerevisiae*, *Biochemistry*, 2011, **50**, 2660-2671.
28. G.P. Holmes-Hampton, R. Miao, J.G. Morales, Y. Guo, E. Münck, and P.A. Lindahl, A nonheme high-spin ferrous pool in mitochondria isolated from fermenting *Saccharomyces cerevisiae*, *Biochemistry*, 2010, **49**, 4227-4234.
29. E.A. Preteasa, G. Schianchi, and D.C. Giori, EPR detection of possible superparamagnetic polyiron nanoparticles and free radicals in the blood serum of patients with homozygous β -thalassemia, *Appl. Magn. Reson.* 2014, **45**, 537-571.
30. R. Miao, M. Martino, J.G. Morales, H. Kim, E.A. Ellis, R. Lill, M.P. Hendrich, E. Münck, P.A. and Lindahl, EPR and Mössbauer spectroscopy of intact mitochondria isolated from Yah1p-depleted *Saccharomyces cerevisiae*, *Biochemistry* 2008, **47**, 9888-9899.
31. R. Miao, H. Kim, U.M.K. Koppolu, E.A. Ellis, R.A. Scott, and P.A. Lindahl, Biophysical characterization of the iron in mitochondria from Atm1p-depleted *Saccharomyces cerevisiae*, *Biochemistry*, 2009, **48**, 9556-9568.
32. J.D. Wofford and P.A. Lindahl, Mitochondrial iron-sulfur-cluster activity and cytosolic iron regulate iron traffic in *Saccharomyces cerevisiae*, *J. Biol. Chem.*, 2015, **290**, 26968-26977.

- 1
2
3 33. A.L. Cockrell, G.P. Holmes-Hampton, S.P. McCormick, M. Chakrabarti, and P.A.
4
5 Lindahl, Mössbauer and EPR study of iron in vacuoles from fermenting *Saccharomyces*
6
7 *cerevisiae*, *Biochemistry*, 2011, **50**, 10275–10283.
8
9
10 34. O.R. Homann, J. Dea, S.M. Noble, and A.D. Johnson, A phenotypic profile of the
11
12 *Candida albicans* regulatory network, *PLOS Genetics*, 2009, **5**, 1-12.
13
14
15 35. J. Park, S.P. McCormick, A.L., Cockrell, M. Chakrabarti, and P.A. Lindahl, High-spin
16
17 ferric ions in *Saccharomyces cerevisiae* vacuoles are reduced to the ferrous state during adenine-
18
19 precursor detoxification, *Biochemistry* 2014, **53**, 3940-3951.
20
21
22 36. D. Blair and H. Diehl, Bathophenanthrolinedisulphonic acid and
23
24 bathocuproinedisulphonic acid, water soluble reagents for iron and copper, *Talanta*, 1961, **7**,
25
26 163-174.
27
28
29 37. J.C. Kapteyn, R.C. Montijn, E., Vink, J. delaCruz, A. Llobell, J.E. Douwes, H. Shimoï,
30
31 P.N. Lipke, and F.M. Klis, Retention of *Saccharomyces cerevisiae* cell wall proteins through a
32
33 phosphodiester-linked beta-1,3-/beta-1,6-glucan heteropolymer, *Glycobiology*, 1996, **6**, 337-
34
35 345.
36
37
38 38. A. Omoike, J. Chorover, K.D. Kwon, and J.D. Kubicki, Adhesion of bacterial
39
40 expolymers to alpha-FeOOH: Inner sphere complexation of phosphodiester groups, *Langmur*,
41
42 2004, **20**, 11108-11114.
43
44
45 39. E. Lesuisse, F. Raguzzi, and R.R. Crichton, Iron uptake by the yeast *Saccharomyces*
46
47 *cerevisiae* – involvement of a reduction step, *J. Gen. Microbiol.*, 1987, **133**, 3229-3236.
48
49
50 40. D.J. Kosman, Redox cycling in iron uptake, efflux and trafficking, *J. Biol. Chem.*, 2010,
51
52 **285**, 26729-26735.
53
54
55
56
57
58
59
60

- 1
2
3 41. A.L. Hughes and D.E. Gottschling, An early age increase in vacuolar pH limits
4 mitochondrial function and lifespan in yeast, *Nature*, 2012, **492**, 261-265.
5
6
7
8 42. Y. Yamaguchi-Iwai, A. Dancis, and R.D. Klausner, AFT1: a mediator of iron regulated
9 transcriptional control in *Saccharomyces cerevisiae*, *EMBO J.*, 1995, **14**, 1231-1239.
10
11
12 43. R.F. Hassett, A.M. Romeo, and D.J. Kosman, Regulation of high affinity iron uptake in
13 the yeast *Saccharomyces cerevisiae* – role of dioxygen and Fe(II), *J. Biol. Chem.*, 1998, **273**,
14 7628-7636.
15
16
17
18 44. J.W. Kronstad, G. Hu, and W.H. Jung, An encapsulation of iron homeostasis and
19 virulence in *Cryptococcus neoformans*, *Trends Microbiol.*, 2013, **21**, 457-465.
20
21
22 45. V.K. Srivastava, K.J. Suneetha, and R. Kaur, A systematic analysis reveals an essential
23 role for high-affinity iron uptake system, haemolysin and CFEM domain-containing protein in
24 iron homeostasis and virulence in *Candida glabrata*, *Biochem. J.*, 2014, **463**, 103-114.
25
26
27
28
29
30
31
32
33

34 **Electronic Supplementary Information:** Table S1: Media composition; Table S2: Final OD₆₀₀
35 and final Fe concentration of cells harvested during media switch experiments; Appendix A:
36 RMSD considerations; Appendix B: propagation of iron concentrations with divisions; Table S3:
37 MB spectral decompositions; Figure S1: UV-Vis spectra of Fe^{II}(BPS)₃ solution and whole yeast
38 cells; Figure S2: changes in percentages of Fe species found in MB spectra of ⁵⁷Fe₄₀B₀ cells
39 transferred to Fe₀B₁₀₀ medium.
40
41
42
43
44
45
46
47
48
49

50 ¹**Abbreviations:** ANU, arbitrary nutrient units; BPS, bathophenanthroline disulfonate; Cell_A,
51 active cells in the math model; Cell_D, dormant cells in the math model; CD, Central doublet
52 representing [Fe₄S₄]²⁺ clusters and LS Fe^{II} heme centers, mainly located in mitochondria; CW,
53
54
55
56
57
58
59
60

1
2
3 cell wall; **DT**, doubling time; **DW**, sterile deionized water; **EDTA**, ethylenediaminetetraacetate;
4
5 **EGTA**, ethylene glycol tetraacetate; $^{57}\text{Fe}_{40}\text{B}_0$, MM with 40 μM $^{57}\text{Fe}^{\text{III}}$ citrate; $^{56}\text{Fe}_{40}\text{B}_0$, same but
6
7 with $^{56}\text{Fe}^{\text{III}}$ citrate; $^{57}\text{Fe}_1\text{B}_{21}$, MM with 1 μM $^{57}\text{Fe}^{\text{III}}$ citrate and 21 μM BPS; Fe_0B_{30} , MM with 30
8
9 μM BPS; $\text{Fe}_0\text{B}_{100}$, MM with 100 μM BPS; Fe_0B_0 , MM; $\text{Fe}_0\text{B}_{100}\text{-NAB}$, MM with 100 μM BPS
10
11 but no amino acids or bases; **GPI**, β -1,6-glucan glycosylphosphatidylinositol; **ICP-MS**,
12
13 inductively coupled plasma mass spectrometer or spectrometry; **LS**, low-spin; **MB**, Mössbauer;
14
15 **MM**, minimal medium; **N**, nutrient component in the math model; **NHHS**, nonheme high-spin;
16
17 **OD₆₀₀**, optical density at 600 nm; **ODE**, ordinary differential equation; **RMSD**, root-mean-
18
19 square deviation; **SP**, sorbitol-phosphate; **TEM**, transmission electron microscopy; **YPAD**, same
20
21 as YPD but with 100 μM added adenine; **YPD**, yeast extract, peptide and dextrose medium.
22
23
24
25
26
27
28
29

30 Figure Legends

31
32 **FIGURE 1. Low field (0.05 T) low temperature (5 K) Mössbauer spectra of whole intact**
33
34 **fermenting WT cells grown on $^{57}\text{Fe}_{40}\text{B}_0$ medium and harvested at different growth stages.**

35
36 A, harvested at $\text{OD}_{600} = 0.4$ (exponential stage) and washed with water; B, harvested at $\text{OD}_{600} =$
37
38 0.7 (exponential stage) and washed with water; C, same as B except treated with lyticase/EDTA;
39
40 D, black hash-marks, harvested at $\text{OD}_{600} = 1.5$ (post-exponential stage; 5 days) and water
41
42 washed; E, same as D except washed with EDTA; F, same as D and E except treated with
43
44 lyticase/EDTA. Red and blue hashmarks in D are the same spectra as shown in E and F,
45
46 respectively, scaled to the spectrum in black. Solid red line in A is a simulation consisting of
47
48 NHHS $S = 5/2$ Fe^{III} from vacuoles (green line; 74%; $\delta = 0.41$ mm/s; $\Delta E_Q = 0.3$ mm/s; $A_{\text{iso}}/g_n\beta_n =$
49
50 -228 kG; $D = 0.5$ cm^{-1} ; $E/D = 0.33$; $\eta = 3$; $\Gamma = 0.7$ mm/s), HS Heme Fe^{II} (orange line: $\delta = 0.8$
51
52 mm/s; $\Delta E_Q = 2.4$ mm/s; $\Gamma = 0.3$ mm/s), central doublet (gold line: $\delta = 0.45$ mm/s; $\Delta E_Q = 1.15$
53
54
55
56
57
58
59
60

1
2
3 mm/s; $\Gamma = 0.7$ mm/s), and NHHS Fe^{II} (purple line: $\delta = 1.26$ mm/s; $\Delta E_Q = 3.0$ mm/s; $\Gamma = 0.6$
4
5 mm/s). The Y-axis scale for A, B, and C are the same.
6
7
8
9

10 **FIGURE 2. 10 K X-Band EPR spectra of whole intact fermenting yeast cells.** A, treated
11 with water; B, treated with EDTA; C, treated with EDTA/lyticase. Other EPR conditions:
12
13 microwave power, 0.2 mW; microwave frequency, 9.645 GHz; modulation amplitude, 9.2 G;
14
15 sweep time, 160 sec. Samples were the same as those used to generate Figure 1 D, E, and F,
16
17 respectively, obtained by transferring samples from MB holder to EPR tubes while maintained
18
19 near 77 K.
20
21
22
23
24
25
26

27 **FIGURE 3. Model of cell growth and O₂ consumption in a batch culture of WT**
28 **fermenting *S. cerevisiae*.** Upper panel: plots of OD₆₀₀ and [O₂] in ⁵⁷Fe₄₀B₀ medium vs. time
29 after inoculation. Data are solid green (OD₆₀₀) and red (O₂) circles. Simulations are green (total
30 cells), yellow (active cells), black (dormant cells), blue (nutrient concentration) and red (O₂
31 concentration) lines. Lower panel: chemical model showing generation of O₂, consumption of O₂
32 by active cells, self-replication of active cells, and interconversion of active and dormant cells as
33 regulated by the nutrient concentration.
34
35
36
37
38
39
40
41
42
43
44
45

46 **FIGURE 4. Temperature-dependent Mössbauer spectra of ⁵⁷Fe-loaded cells (water**
47 **washed).** A, 5; B, 15; C, 25; D, 50; E, 75; F, 100; G, 150 (all in K). A field of 0.05 T was applied
48 parallel to the gamma radiation. The sample used was the same as in Figure 1D. Overall
49 simulations (red lines in A and F) were the sum of two simulated spectra, including an S = 5/2
50 species ($A_{\text{iso}}/g_n\beta_n = -216$ kG, $D = 0.04$ cm⁻¹, $E/D = 0.22$, $\delta = 0.45$ mm/s, $\Delta E_Q = 0.5$ mm/s, $\eta = 10$
51
52
53
54
55
56
57
58
59
60

1
2
3 and $\Gamma = 0.4 - 0.7$ mm/s) representing 70% of spectral intensity, and an $S = 0$ species ($\delta = 0.38$
4 mm/s, $\Delta E_Q = 0.5$ mm/s, $\eta = 1$ and $\Gamma = 0.4 - 0.7$ mm/s) representing 30% of spectral intensity.
5
6
7
8 With increasing temperature, spectral features broadened.
9

10
11
12 **FIGURE 5. Variable-Field 4.2 K Mössbauer spectra of ^{57}Fe -loaded (water washed) cells.**
13
14 A, 0; B, 0.75; C, 1.5; D, 3.0, and E, 6.0 (all in T). Fields were applied perpendicular to the
15 gamma radiation. Overall simulations (red lines) were generated using the same model as in the
16 Figure 4 legend. The sample was the same as used in Figures 1D and 4. The simulation in A
17 assumed an applied field of 0.02 T and that the sextet represented 65% of spectral intensity and
18 the doublet 35%.
19
20
21
22
23
24
25
26
27
28
29

30 **FIGURE 6. Temperature-dependent EPR spectra of ^{57}Fe -loaded cells (water washed).**
31
32 Low-field spectra show the $g = 4.3$ signal while high-field spectra exhibit a broad $g = 2$ signal.
33
34 Spectra were collected at 10 K (red line), 20 K (yellow), 40 K (green), and 80 K (blue). Signal
35 intensities have been multiplied by temperature. The sample used was the same as in Figure 1D,
36
37 4 and 5. Microwave power was 2 mW and 0.2 mW for the low- and high-field spectra,
38
39 respectively. Other conditions were as in Figure 2.
40
41
42
43
44
45

46 **FIGURE 7. Iron concentrations in WT post-exponential cells and the corresponding**
47 **washes after various treatments.** A, $[\text{Fe}]_{\text{cell}}$; B, $[\text{Fe}]_{\text{wash}}$. Data are solid circles. Black, washed
48 with water only; Red, washed with EDTA only; Blue, washed with lyticase and EDTA.
49
50
51
52
53
54
55
56
57
58
59
60

1
2
3 **FIGURE 8. Panel A, Growth of Fe-loaded or Fe-starved Cells after transfer to various**
4 **media.** Solid circles, Fe-loaded cells transferred to Fe_0B_{30} medium. Open circles, Fe-starved
5 cells transferred to Fe_0B_{30} medium. Solid triangles, Fe-loaded cells transferred to $\text{Fe}_0\text{B}_{100}$. Open
6 triangles, Fe-starved cells transferred to $\text{Fe}_0\text{B}_{100}$ medium. **Panel B, Growth of Fe-loaded cells**
7 **transferred to various media inoculated at conserved cell density.** Solid squares, transferred
8 to $^{57}\text{Fe}_{40}\text{B}_0$ medium. Open squares, transferred to $\text{Fe}_0\text{B}_{100}$ medium. Crosses, transferred to
9 $\text{Fe}_0\text{B}_{100}$ -NAB medium. **Panel C, same as Panel B, but a different experiment.** Solid squares,
10 transferred to $^{56}\text{Fe}_{40}\text{B}_0$ medium. Open squares, transferred to $\text{Fe}_0\text{B}_{100}$ medium. Solid diamonds,
11 transferred to Fe_0B_0 medium. Open diamonds, transferred to DW.
12
13
14
15
16
17
18
19
20
21
22
23
24
25
26

27 **FIGURE 9. Mössbauer spectra (5 K, 0.05 T) of whole WT yeast cells before (A) and after**
28 **(B – E) switching growth media.** Results from this experiment are also presented in Figure 8B.
29 **A,** Fe-loaded cells. The blue line is a simulation of Fe^{III} nanoparticles ($\delta = 0.53$ mm/s; $\Delta E_Q =$
30 0.52 mm/s; $\Gamma = 0.45$ mm/s). The red line is a composite simulation including 20% absorption
31 due to nanoparticles and 65% to NHHS Fe^{III} ($A_{\text{iso}}/g_n\beta_n = -235$ kG; $E/D = 0.33$; $D = 1.15$ cm $^{-1}$; δ
32 $= 0.55$ mm/s; $\Delta E_Q = 0$ mm/s; $\Gamma = 0.8$ mm/s). **B,** Fe-loaded cells 5 days after being transferred to
33 $\text{Fe}_0\text{B}_{100}$. Red line is a composite simulation including NHHS Fe^{III} and the quadrupole doublet
34 due to $^{57}\text{Fe}^{\text{II}}(\text{BPS})_3$. Simulation parameters are given in Table S3. **C,** same as B but after
35 removing the quadrupole doublet due to $^{57}\text{Fe}^{\text{II}}(\text{BPS})_3$. The green line is a simulation of the
36 NHHS Fe^{II} doublet and the red line is a composite simulation defined in Table S3. **D,** Fe-loaded
37 cells 1 day after being transferred to $\text{Fe}_0\text{B}_{100}$ -NAB medium. Red line is a composite simulation.
38 **E,** same as D but after removing the quadrupole doublet due to $\text{Fe}^{\text{II}}(\text{BPS})_3$. Green and maroon
39
40
41
42
43
44
45
46
47
48
49
50
51
52
53
54
55
56
57
58
59
60

lines are simulations of the two NHHS Fe^{II} species described in the text. The red line is a composite simulation.

FIGURE 10. Iron concentrations in growth medium before and after inoculation with ⁵⁷Fe-loaded cells. Other results of this experiment are presented in Figure 1C. **Panel A, ⁵⁷Fe concentration in media:** Solid squares, medium before and after ⁵⁷Fe-loaded cells were transferred to Fe₀B₁₀₀ medium. The datum at t < 0 was of medium prior to inoculation. Other data are of the medium 0, 6, 12 and 24 hr after the transfer and after cells were removed by centrifugation. Solid triangles, same but for Fe₀B₀ medium. Blank circles, same but for DW. **Panel B, Fe concentration in ⁵⁶Fe₄₀B₀ medium:** Solid circles, total [Fe]; Open diamonds, [⁵⁶Fe]; Solid diamonds [⁵⁷Fe].

FIGURE 11. Whole-cell Mössbauer spectra (5 K, 0.05 T) obtained from the experiment of Figure 8C. A, ⁵⁷Fe-loaded cells; B – F, ⁵⁷Fe-loaded cells after 1 day incubation in the following media: B, Fe₀B₀; C, DW; D, Fe₀B₁₀₀; E, same as D, but cells were rinsed with 100 mM Tris-HCl buffer (pH 9.4) three times prior to obtaining the spectrum; F, ⁵⁶Fe₄₀B₀. Red and blue lines in A and C are the same as in Figure 9A. The green line in B simulates the CD while the red line is a composite simulation as defined in Table S3. The red line in D simulates the Fe^{II}(BPS)₃ doublet, the green line in E simulates the CD, and the orange line in F simulates the NHHS Fe^{II} doublet.

FIGURE 12. Mössbauer spectra (5 K, 0.05 T) of ⁵⁷Fe-loaded cells before (A) and at increasing times after (B – E) transfer to Fe₀B₁₀₀ medium. Time after transfer: B, 30 min; C, 3 hr; D, 6 hr. Blue and pink lines are simulations of the Fe^{III} nanoparticle and Fe^{II}(BPS)₃

1
2
3 quadrupole doublets, respectively. The red lines are composite simulations as defined in Table
4
5 S3. The arrow in B indicates the position of the high energy line of the NHHS Fe^{II} doublet.
6
7
8
9

10 **FIGURE 13. Western Blot showing Fet3p expression levels in WT cells in various media.**

11
12 Top panel, Fe-loaded cells transferred to Fe_{e40}B₀, ⁵⁶Fe₄₀B₀, and Fe₀B₀ media and harvested at the
13
14 indicated times (in hr) after the transfer. Bottom panel, same as top panel but with cells
15
16 transferred to Fe₀B₁₀₀ and DW media.
17
18
19
20
21

22 **FIGURE 14. Model for iron accumulation into the cell wall.** Metabolically active

23 (exponentially-growing) cells do not accumulate Fe in their CWs; Fe^{III} from the environment is
24
25 reduced by metabolic processes in the cell and it enters the cell as Fe^{II}. As cells transition into a
26
27 post-exponential (or dormant) state, Fe^{III} begins to accumulate in the CW. CW Fe can be
28
29 removed by chelation or CW digestion. When dormant cells become metabolically active (by
30
31 placing them into fresh media), the CW Fe^{III} becomes reductively mobilized to the Fe^{II} state. The
32
33 Fe^{II} is released from the CW where it can: a) dissociate from the cell and diffuse into the
34
35 environment; b) enter the cytosol to support cell growth; or c) chelate with BPS (if BPS is in the
36
37 medium). A significant portion of the neutral Fe^{II}(BPS)₃ species adsorbs onto the CW.
38
39
40
41
42
43
44
45
46
47
48
49
50
51
52
53
54
55
56
57
58
59
60

Table 1. Metal concentrations of WT cells grown to exponential and post-exponential phases, and subsequently treated with EDTA or lyticase. Concentrations are in μM .

| OD ₆₀₀ | Treatment | [Fe] | [Mn] | [Cu] | [Zn] |
|-------------------|---------------|------|------|------|------|
| 0.2 | Water | 230 | 14 | 22 | 320 |
| 0.4 | Water | 190 | 12 | 24 | 440 |
| 0.7 | Water | 590 | 10 | 24 | 560 |
| 0.7 | Lyticase/EDTA | 480 | 13 | 21 | 420 |
| 1.5 | Water | 7400 | 12 | 32 | 620 |
| 1.6 | EDTA | 4400 | 9 | 24 | 510 |
| 1.5 | Lyticase/EDTA | 1800 | 8 | 30 | 600 |

Table 2. Model Reactions, Parameters and Sensitivities. Sensitivities were determined as described (32). 1250 is the maximum concentration (in μM) of dissolved O_2 in the medium. The rate of O_2 increase in the medium at any time was assumed to be proportional to the difference between 1250 μM and the concentration of dissolved O_2 at that time. This arrangement prevented $[\text{O}_2]$ from exceeding the known saturation limit of O_2 . ANU, arbitrary nutrient units.

| Reaction | Rate Expression | Parameter | Sensitivity |
|---|--|---|----------------------|
| $N \xrightarrow{R_a} \text{Cell}_A$ | $R_a = k_a \cdot [N] \cdot [\text{Cell}_A]$ | $k_a = 0.18 \text{ hr}^{-1} \text{ ANU}^{-1}$ | 1.08 |
| $\text{O}_2 \xrightarrow{R_m}$ | $R_m = k_m \cdot [\text{O}_2] \cdot [\text{Cell}_A]$ | $k_m = 690 \text{ hr}^{-1} \text{ OD}^{-1}$ | 1.04 |
| $\text{Cell}_A \xrightarrow{R_d} \text{Cell}_D$ | $R_d = k_d \cdot \left(\frac{1}{1 + \left(\frac{[N]}{[N]_{sp}} \right)^{sen}} \right) [\text{Cell}_A]$ | $k_d = 0.072 \text{ hr}^{-1}$ $[N]_{sp} = 0.01 \text{ ANU}$ $sen = 6.6$ | 1.01 1.00 1.00 |
| $\xrightarrow{R_o} \text{O}_2$ | $R_o = k_o \cdot (1250 - [\text{O}_2])$ | $k_o = 220 \text{ hr}^{-1}$ | 1.01 |
| $\text{Cell}_D \xrightarrow{R_b} \text{Cell}_A$ | $R_b = k_b \cdot \left(1 - \frac{1}{1 + \left(\frac{[N]}{[N]_{sp}} \right)^{sen}} \right) [\text{Cell}_D]$ | $k_b = 0.33 \text{ hr}^{-1}$ | 1.00 |

Figure 1

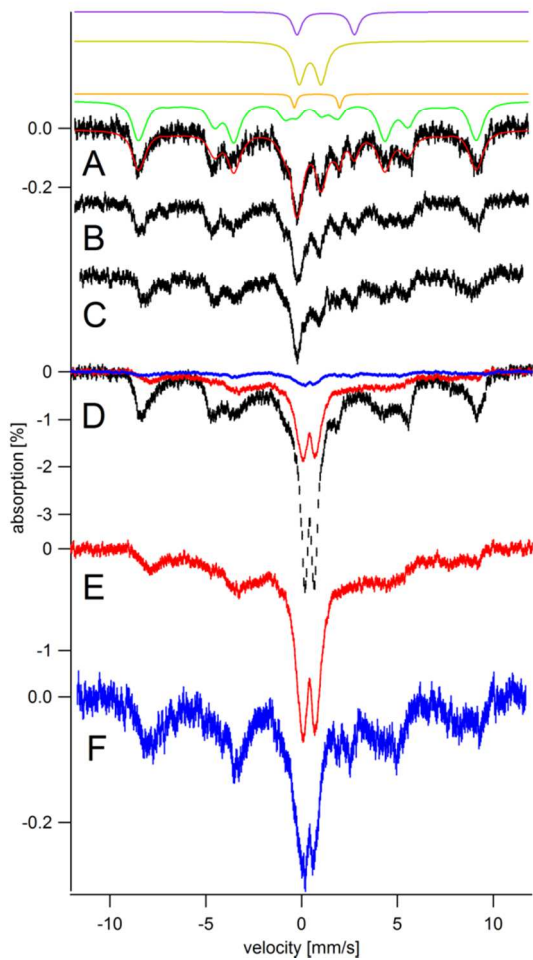
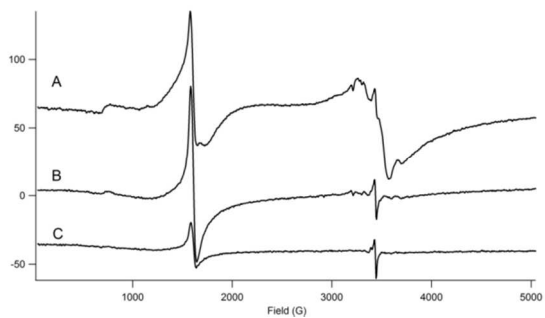


Figure 2



1
2
3
4
5
6
7
8
9
10
11
12
13
14
15
16
17
18
19
20
21
22
23
24
25
26
27
28
29
30
31
32
33
34
35
36
37
38
39
40
41
42
43
44
45
46
47
48
49
50
51
52
53
54
55
56
57
58
59
60

Figure 3

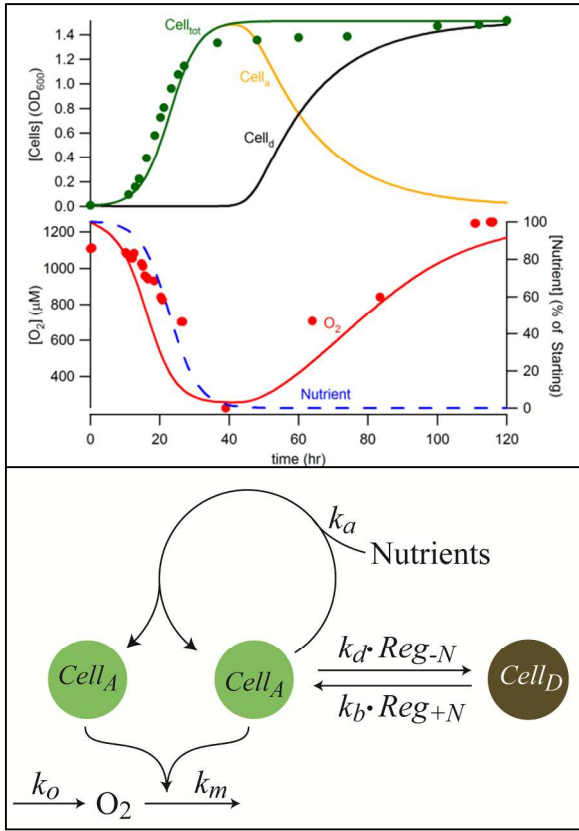


Figure 4

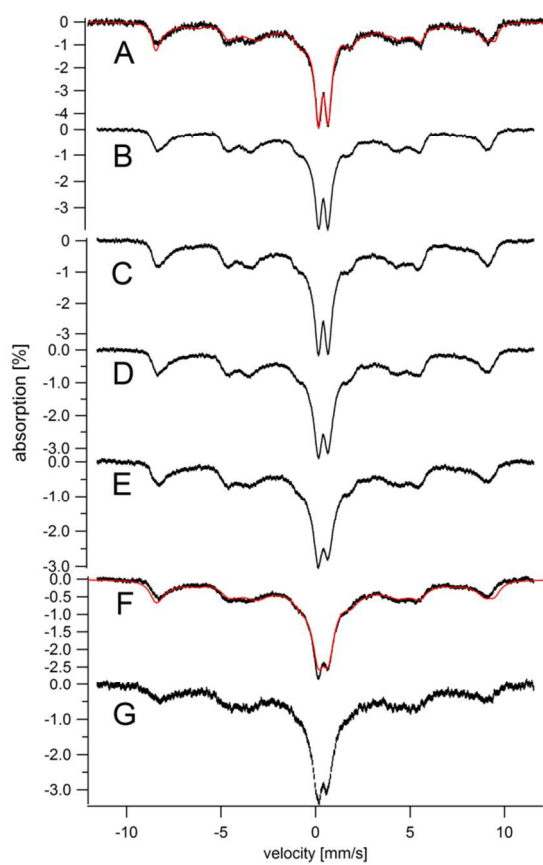


Figure 5

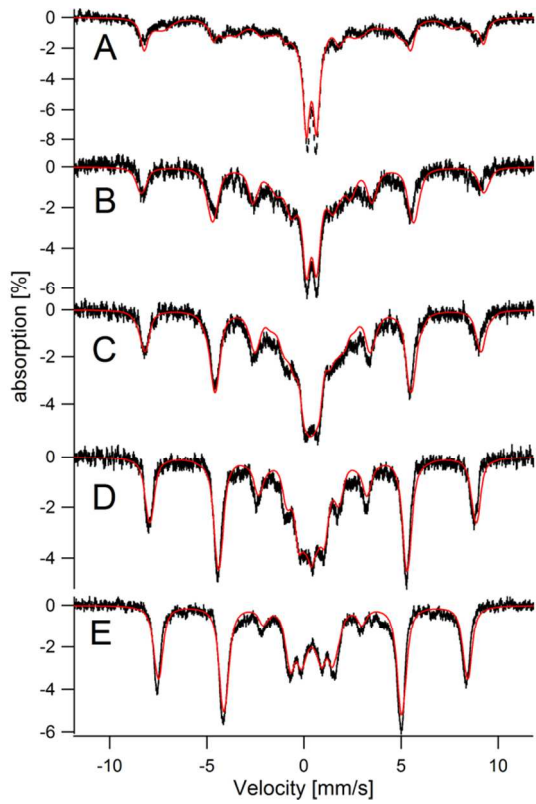
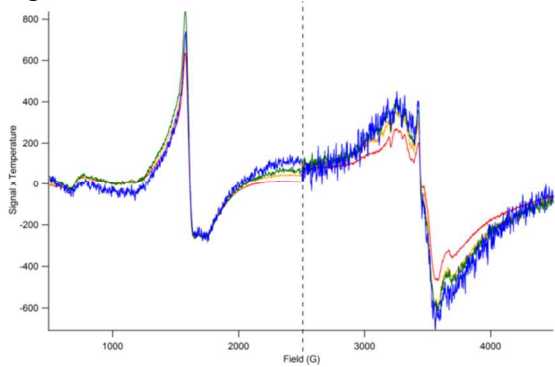


Figure 6



1
2
3
4
5
6
7
8
9
10
11
12
13
14
15
16
17
18
19
20
21
22
23
24
25
26
27
28
29
30
31
32
33
34
35
36
37
38
39
40
41
42
43
44
45
46
47
48
49
50
51
52
53
54
55
56
57
58
59
60

Figure 7

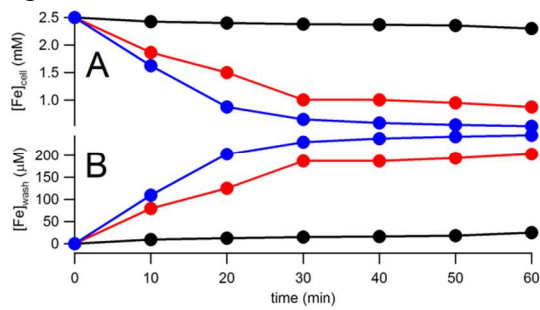


Figure 8

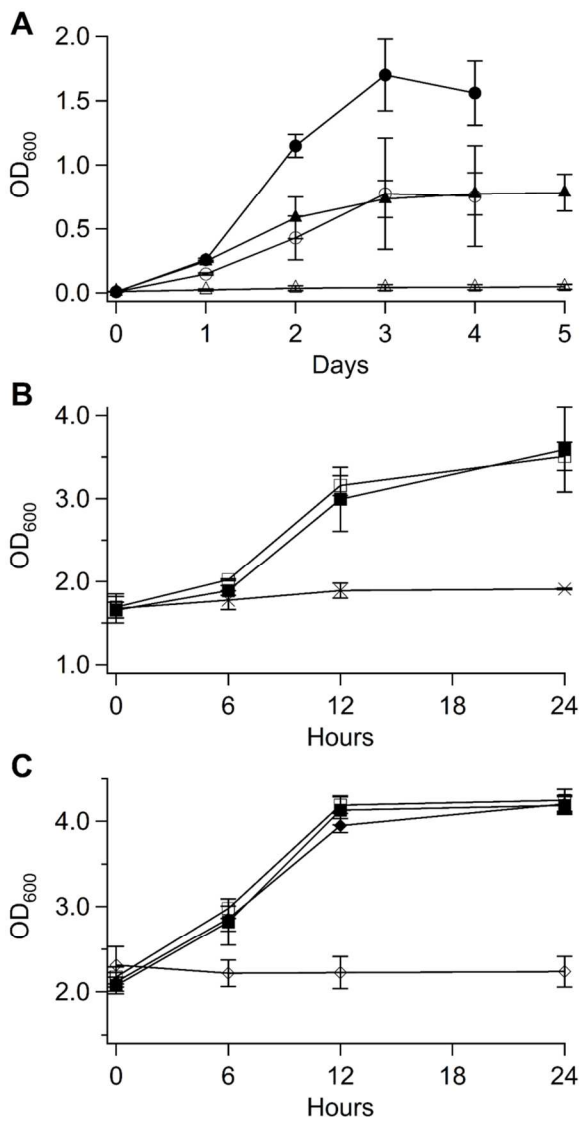


Figure 9

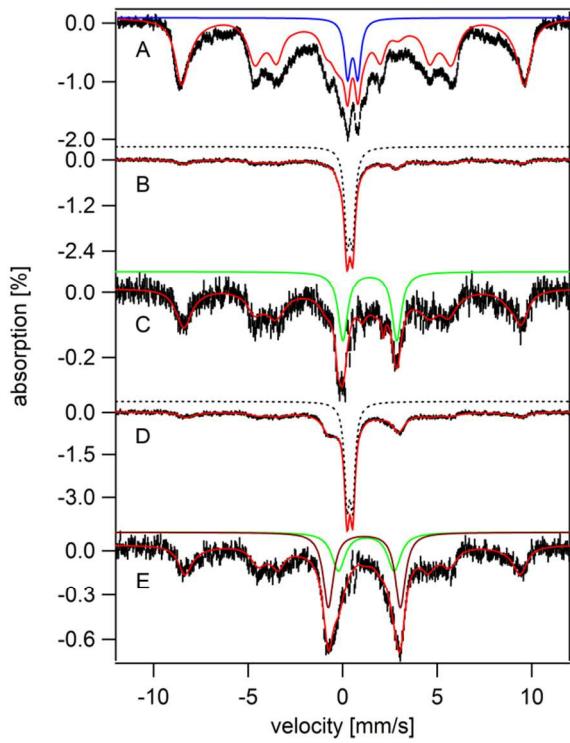


Figure 10

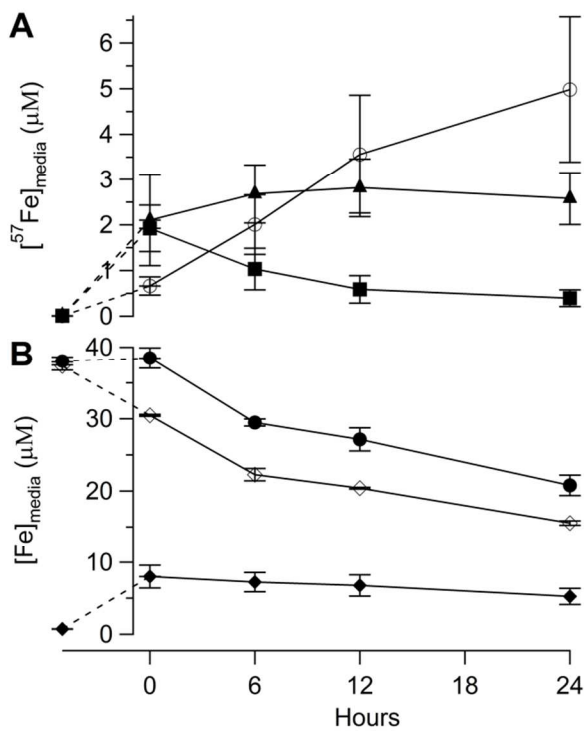
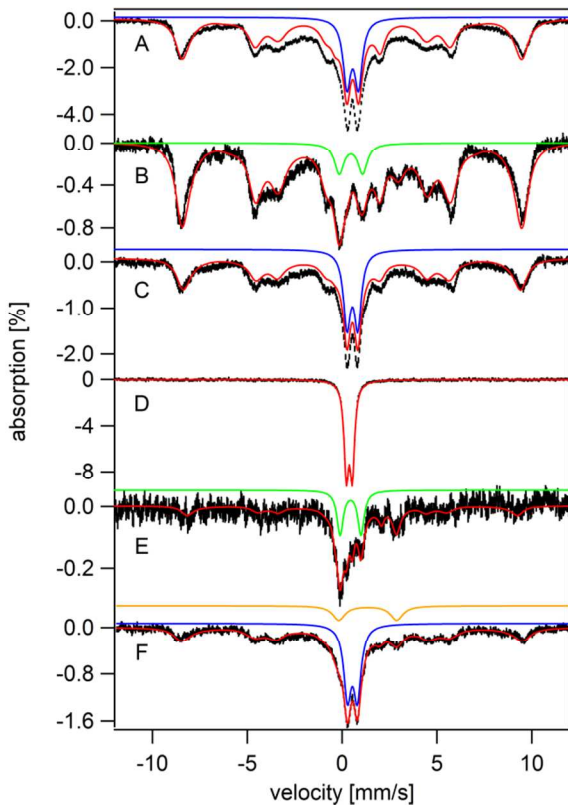


Figure 11



1
2
3
4
5
6
7
8
9
10
11
12
13
14
15
16
17
18
19
20
21
22
23
24
25
26
27
28
29
30
31
32
33
34
35
36
37
38
39
40
41
42
43
44
45
46
47
48
49
50
51
52
53
54
55
56
57
58
59
60

Figure 12

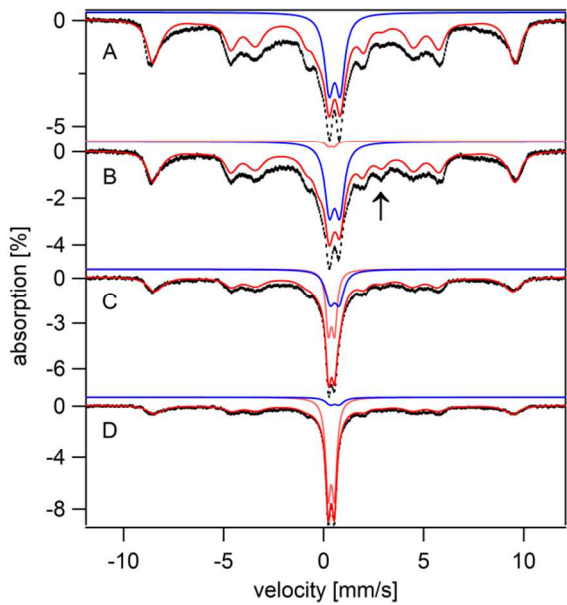
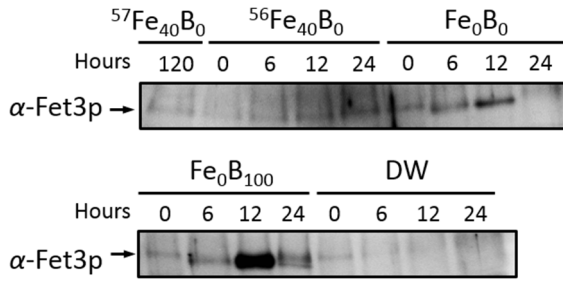


Figure 13



1
2
3
4
5
6
7
8
9
10
11
12
13
14
15
16
17
18
19
20
21
22
23
24
25
26
27
28
29
30
31
32
33
34
35
36
37
38
39
40
41
42
43
44
45
46
47
48
49
50
51
52
53
54
55
56
57
58
59
60

Figure 14

